Inorganic Chemistry

Article

pubs.acs.org/IC

Hydroxide-Bridged Cubane Complexes of Nickel(II) and Cadmium(II): Magnetic, EPR, and Unusual Dynamic Properties

Daniel L. Reger,*[,†] Andrea E. Pascui,[†] Perry J. Pellechia,[†] Mark D. Smith,[†] Julia Jezierska,[‡] and Andrew Ozarowski*[,§]

[†]Department of Chemistry and Biochemistry, University of South Carolina, Columbia, South Carolina 29208, United States

[‡]Faculty of Chemistry, University of Wrocław, 50-383 Wrocław, Poland

[§]National High Magnetic Field Laboratory, Florida State University, Tallahassee, Florida 32310, United States

Supporting Information

ABSTRACT: The reactions of $M(ClO_4)_2 \cdot xH_2O$ (M = Ni(II) or Cd(II)) and *m*-bis[bis(1-pyrazolyl)methyl]benzene ($\mathbf{L_m}$) in the presence of triethylamine lead to the formation of hydroxide-bridged cubane compounds of the formula $[M_4(\mu_3\text{-}OH)_4(\mu\text{-}\mathbf{L_m})_2(solvent)_4](ClO_4)_4$, where solvent = dimethylformamide, water, acetone. In the solid state the metal centers are in an octahedral coordination environment, two sites are occupied by pyrazolyl nitrogens from $\mathbf{L_m}$, three sites are occupied by bridging hydroxides, and one site contains a weakly coordinated solvent molecule. A series of multinuclear, two-dimensional and variable-temperature NMR experiments showed that the cadmium(II) compound in acetonitrile-d_3 has C_2 symmetry and undergoes an unusual dynamic process at higher temperatures ($\Delta G^{\ddagger}_{Lm}$ = 15.8 ± 0.8 kcal/mol at 25 °C) that equilibrates the pyrazolyl rings, the hydroxide hydrogens, and cadmium(II) centers. The proposed mechanism for this process combines two motions in the semirigid $\mathbf{L_m}$ ligand termed the "Columbia Twist and Flip:" twisting of the pyrazolyl rings along the $C_{pz}-C_{methine}$ bond and 180° ring flip of the phenylene spacer along the $C_{Ph}-C_{methine}$ bond. This dynamic process was also followed using the spin saturation method, as was the exchange of the hydroxide hydrogens with the trace water present in acetonitrile-d_3. The nickel(II) analogue, as shown by magnetic susceptibility and electron paramagnetic resonance measurements, has an $S = 4$ ground state, and the nickel(II) centers are ferromagnetically coupled with strongly nonaxial zero-field splitting parameters. Depending on the Ni−O−Ni angles two types of interactions are observed: J_1 = 9.1 cm^{-1} (97.9 to 99.5°) and J_2 = 2.1 cm^{-1} (from 100.3 to 101.5°). "Broken symmetry" density functional theory calculations performed on a model of the nickel(II) compound support these observations.

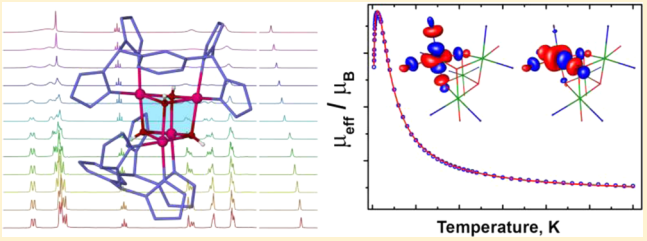

INTRODUCTION

Polynuclear complexes of magnetic metal centers are viable candidates for applications in various fields, as biomimetic systems used for the study of enzyme active sites and multielectron transfers[1] or as magnetic materials for applications in the field of molecular nanotechnology.[2] The magnetic exchange between paramagnetic metal ions is important not only from a theoretical point of view,[3] which aims to understand the fundamental correlation between the structure and magnetic properties, but also targets the development of single-molecule magnets (SMM).[4] One promising motif for SMM is based on nickel-hydroxy cubane-type tetrametallic clusters, which recently received increased attention.[5]

In these systems the metallic centers are usually in an octahedral coordination environment, where three sites are occupied by small bridging atoms. The literature presents two types of cubane core clusters supported by polydentate ligands with oxygen and/or nitrogen donors:[5,6] (i) donor atoms in the polydentate ligand occupy the bridging cubane positions, each bridging three metal centers—depending on the nature of the ligand, the remaining metal sites are occupied by other ligand donor atoms, anions, or solvent molecules; (ii) more commonly the sole role of the ligand is to stabilize the coordination sphere of the metal centers, the core is generated by triply bridged anions, especially methoxide or other small ligands such as azide, halides, sulfides, and hydroxide.

Herein we report nickel(II) and cadmium(II) cubane-core tetrametallic compounds of the second type with triply bridging hydroxide linking the metal centers. This core is stabilized by third-generation, ditopic bis(pyrazolyl)methane ligands. There are only a few magnetically characterized structures known where the nickel(II) cubane core is generated by triple bridging of the hydroxide groups,[6] and no analogous cadmium(II) compounds were found in the literature. The small number of cubane-core cadmium(II) compounds that are known contain triple bridging chloride[7] and di-2-pyridyl ketone and/or carboxylates.[8]

We have recently synthesized a series of monofluoride-bridged dinuclear metallacyclic compounds of the type $[M_2(\mu$-

Received: December 10, 2013
Published: April 21, 2014

   dx.doi.org/10.1021/ic403013d | Inorg. Chem. 2014, 53, 4325−4339

F)(μ-$\mathbf{L_m}$)$_2$](BF$_4$)$_3$, M = Fe(II), Co(II), Cu(II), Zn(II), where $\mathbf{L_m}$ is *m*-bis[bis(1-pyrazolyl)methyl]benzene (*m*-[CH(pz)$_2$]$_2$C$_6$H$_4$, pz = pyrazolyl ring, Scheme 1).[9] Interestingly,

Scheme 1. Schematic Drawing of the Structure of $\mathbf{L_m}$

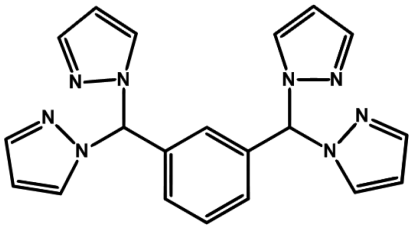

syntheses analogous to those used in these preparations with the metals nickel(II) and cadmium(II) generated *difluoride*-bridged compounds, [M$_2$(μ-F)$_2$(μ-$\mathbf{L_m}$)$_2$](BF$_4$)$_2$.

We have also prepared the analogous hydroxide-bridged complexes [M$_2$(μ-OH)(μ-$\mathbf{L_m}$)$_2$](ClO$_4$)$_3$, (M = Fe(II), Co(II), Cu(II), Zn(II)) using triethylamine as the base to generate the hydroxide ligands from water molecules present in the syntheses.[10] As observed with the fluoride-bridged complexes, we report here that analogous reactions where M = Ni(II) or Cd(II) lead to different types of products, the cubane-core hydroxide-bridged complexes [Ni$_4$(μ_3-OH)$_4$(μ-$\mathbf{L_m}$)$_2$(DMF)$_4$](ClO$_4$)$_4$·DMF·EtOH, {Ni$_4$(μ_3-OH)$_4$(μ-$\mathbf{L_m}$)$_2$(DMF)$_2$[(H$_2$O)$_{0.79}$(MeOH)$_{0.21}$]$_2$}(ClO$_4$)$_4$·2(DMF)·2[(MeOH)$_{0.79}$(Et$_2$O)$_{0.21}$], and [Cd$_4$(μ_3-OH)$_4$(μ-$\mathbf{L_m}$)$_2$(acetone)$_2$(H$_2$O)$_2$](ClO$_4$)$_4$·2acetone (DMF = dimethylformamide) as characterized by X-ray crystallography. We studied the magnetic and electron paramagnetic resonance (EPR) properties of the first nickel(II) complex and carried out detailed NMR investigations on the cadmium(II) complex, which shows a unique dynamic behavior in solution.

EXPERIMENTAL SECTION

General Considerations. For the synthesis of the cubane-core compounds standard Schlenk techniques were used. The solvents were not dried prior to use. The ligand $\mathbf{L_m}$ was prepared following reported procedures.[9c] All other chemicals were purchased from Sigma-Aldrich or Strem Chemicals and used as received.

Crystals used for elemental analysis and mass spectrometry were removed from the mother liquor, rinsed with ether, and dried under vacuum.

^{1}H, ^{13}C, and ^{113}Cd NMR spectra were recorded on a Varian Mercury/VX 300, Varian Mercury/VX 400, or Varian INOVA 500 spectrometer on samples that were dried in vacuum. All chemical shifts are in ppm and were referenced to residual undeuterated solvent signals (^{1}H), deuterated solvent signals (^{13}C), or externally to CdCl$_2$ (^{113}Cd). Diffusion measurements were run on a Bruker Avance-DRX 400 MHz NMR spectrometer. The vendor-supplied bipolar pulse pairs−longitudinal encode/decode (BPP-LED) pulse sequence was used with 1 ms gradient pulses and a 300 ms diffusion time. The 16 free induction decay signals (FIDs) with varying gradient strength were collected with 8 scans. Data processing was performed with Bruker Topspin 1.3 using the included diffusion-ordered spectroscopy (DOSY) routine. To test the accuracy of the spin saturation transfer experiment, we used a sample of *N*,*N*-dimethylacetamide diluted in toluene-d_8 and calculated k and $\Delta G^{\ddagger}$ for the rotational barrier about the amide bond. The calculated values (25.0 °C: k = 0.53 s^{-1}, $\Delta G^{\ddagger}$ = 17.8 kcal/mol) are comparable with literature values (22.5 °C: k = 0.61 s^{-1}, $\Delta G^{\ddagger}$ = 17.7 kcal/mol).[11]

Mass spectrometric (MS) measurements were obtained on a MicroMass QTOF spectrometer in an acid-free environment. For all reported peaks, the isotopic patterns match those calculated for the assignments. Elemental analyses were performed on samples dried to constant weight by Robertson Microlit Laboratories (Ledgewood, NJ).

The XSEED,[12] POV-RAY,[12] gOpenMol,[12] and MESTRENOVA[13] computer programs were used for the preparation of figures.

High-field, high-frequency EPR spectra were measured on crystalline samples of **1**, which were not dried in vacuum, at temperatures ranging from ca. 6 to 290 K using a home-built spectrometer at the Electro-Magnetic Reduction (EMR) facility of the National High Magnetic Field Laboratory (NHMFL).[14] The instrument is a transmission-type device in which microwaves are propagated in cylindrical lightpipes. The microwaves were generated by a phase-locked Virginia Diodes source generating frequency of 13 ± 1 GHz and producing its harmonics of which the 2nd, 4th, 6th, 8th, 16th, 24th, and 32nd were available. A superconducting magnet (Oxford Instruments) capable of reaching a field of 17 T was employed. The powder samples were not constrained and showed no magnetic torqueing at high magnetic fields.

Magnetic susceptibility measurements were made on crystalline samples of **1**, which were not dried in vacuum, over the temperature range of 1.8−300 K. They were performed at a magnetic field of 0.5 T using a Quantum Design SQUID MPMSXL-5 magnetometer. Correction for the sample holder, as well as the diamagnetic correction χ_D, which was estimated from the Pascal constants,[15] was applied.

Caution! *Perchlorate salts of metal complexes with organic ligands are potentially explosive.*[16]

[Ni$_4$(μ_3-OH)$_4$(μ-$\mathbf{L_m}$)$_2$(DMF)$_4$](ClO$_4$)$_4$·DMF·EtOH, ***1***. The ligand $\mathbf{L_m}$ (0.444 g, 1.2 mmol) was dissolved in 16 mL of methanol, and then NEt$_3$ (0.17 mL, 1.2 mmol) was added. The Ni(ClO$_4$)$_2$·6H$_2$O (0.439 g, 1.2 mmol) was dissolved in 4 mL of methanol, and the ligand/amine solution was transferred by cannula into the nickel salt solution. The reaction mixture was stirred for 24 h, after which time the system was filtered by cannula. The resulting green solid (0.210 g) was washed with 5 mL of ether and dried in vacuum overnight. Layering a buffer layer of pure EtOH and then Et$_2$O on top of the DMF solution of the crude product afforded 0.100 g of [Ni$_4$(μ-OH)$_4$(μ-$\mathbf{L_m}$)$_2$(DMF)$_4$](ClO$_4$)$_4$·DMF·EtOH single crystals suitable for X-ray studies. Anal. Calcd(Found) for [Ni$_4$(μ-OH)$_4$(μ-$\mathbf{L_m}$)$_2$(DMF)$_4$](ClO$_4$)$_4$, C$_{52}$H$_{68}$Cl$_4$Ni$_4$N$_{20}$O$_{24}$: C, 36.02 (36.25); H, 3.95 (4.22); N, 16.16 (15.90)%. MS electrospray (ES)(+) m/z (rel. % abund.) [assgn]: 1341 (15) [Ni$_4$($\mathbf{L_m}$)$_2$(OH)$_4$(ClO$_4$)$_3$]$^+$, 662 (13) [Ni$_4$($\mathbf{L_m}$)$_2$(OH)$_3$(ClO$_4$)$_3$]$^{2+}$, 621 (100) [Ni$_4$($\mathbf{L_m}$)$_2$(OH)$_4$(ClO$_4$)$_2$]$^{2+}$, 527 (25) [Ni$_2$($\mathbf{L_m}$)$_2$(ClO$_4$)$_2$]$^{2+}$, 445 (7) [Ni$\mathbf{L_m}$OH]$^+$, 378 (80) [Ni$_4$($\mathbf{L_m}$)$_2$(OH)$_4$(ClO$_4$)]$^{3+}$, 371 (22) [$\mathbf{L_m}$ + H]$^+$, 292 (92) [Ni$_2$($\mathbf{L_m}$)$_2$(OH)]$^{3+}$. The use of MeOH instead of EtOH in the crystallization procedure resulted in crystals of {Ni$_4$(μ_3-OH)$_4$(μ-$\mathbf{L_m}$)$_2$(DMF)$_2$[(H$_2$O)$_{0.79}$(MeOH)$_{0.21}$]$_2$}(ClO$_4$)$_4$·2(DMF)·2[(MeOH)$_{0.79}$(Et$_2$O)$_{0.21}$], **2**.

[Cd$_4$(μ_3-OH)$_4$(μ-$\mathbf{L_m}$)$_2$(acetone)$_2$(H$_2$O)$_2$](ClO$_4$)$_4$·2acetone, ***3***. The cadmium(II) compound was synthesized similarly starting from $\mathbf{L_m}$ (0.190 g, 0.514 mmol), NEt$_3$ (0.070 mL, 0.514 mmol), and Cd(ClO$_4$)$_2$·6H$_2$O (0.215 g, 0.514 mmol). Vapor diffusion of Et$_2$O into the diluted acetonitrile solution of the crude product at 5 °C afforded 0.148 g (44%) of transparent single crystals and white microcrystalline solid. ^{1}H NMR (300 MHz, acetonitrile-d_3): 8.40/8.37 (s/s, 2*H*/2H, 5-pz), 8.20/8.16/8.13 (s/s/s, 12H, 5-pz +3-pz + CH(pz)$_2$), 7.56 (t, J = 9 Hz, 2H, 5-H C$_6$H$_4$), 6.94/6.91 (d/s, 6H, 4,6-H C$_6$H$_4$ + 3-pz), 6.76 (d, 2H, 4,6-H C$_6$H$_4$), 6.70 (s, 2H, 4-H pz), 6.52 (s, 6H, 4-H pz), 5.01 (s, 2H, 2-H C$_6$H$_4$), 2.59 (s, 2H, Cd−OH−Cd), −2.11 (s, 2H, Cd−OH−Cd). ^{1}H NMR (400 MHz, acetone-d_3): 8.65 (s br, 8H, 5-pz + C*H*(pz)$_2$), 8.38 (s br, 8H, 5-pz +3-pz), 8.29 (s, 2H, 3-pz), 7.67 (t, J = 8 Hz, 2H, 5-H C$_6$H$_4$), 7.23 (s, 2H, 3-pz), 7.02 (d, 2H, 4,6-H C$_6$H$_4$), 6.84 (d, 2H, 4,6-H C$_6$H$_4$), 6.69 (s, 2H, 4-H pz), 6.58 (s, 6H, 4-H pz), 5.19 (s, 2H, 2-H C$_6$H$_4$), −1.50 (s, 2H, Cd−OH−Cd). ^{13}C NMR (100.6 MHz, acetone-d_6): δ 146.1/145.7/145.0 (5-C pz), 139.0 (1,3-H C$_6$H$_4$), 136.8/136.6/136.2/135.8 (3-C pz), 130.6 (5-C C$_6$H$_4$), 128.8 (4,6-C C$_6$H$_4$), 125.4 (2-C C$_6$H$_4$), 108.1/107.9/107.7/107.6 (4-C pz), 75.2 (CH(pz)$_2$). ^{113}Cd NMR (88.8 MHz, acetone-d_6): δ 3.1/1.7 (s/s). Anal. Calcd (Found) for [Cd$_4$(μ-OH)$_4$(μ-$\mathbf{L_m}$)$_2$](ClO$_4$)$_4$, C$_{40}$H$_{40}$Cl$_4$Cd$_4$N$_{16}$O$_{20}$: C, 29.01 (29.50); H, 2.43 (2.35); N, 13.53 (13.44)%. MS ES(+) m/z (rel. % abund.) [assgn]: 1556 (2) [Cd$_4$($\mathbf{L_m}$)$_2$(OH)$_4$(ClO$_4$)$_3$]$^+$, 1181 (2) [Cd$_2$($\mathbf{L_m}$)$_2$(OH)(ClO$_4$)$_2$]$^+$, 953

dx.doi.org/10.1021/ic403013d | Inorg. Chem. 2014, 53, 4325−4339

(8) $[Cd(\mathbf{L_m})_2(ClO_4)]^+$, 729 (30) $[Cd_4(\mathbf{L_m})_2(OH)_4(ClO_4)_2]^{2+}$, 583 (100) $[Cd(\mathbf{L_m})(ClO_4)]^+$, 519 (90) $[Cd(\mathbf{L_m})(OH)_2 + H]^+$, 501 (15) $[Cd_2(\mathbf{L_m})_2(OH)_2]^{2+}$, 427 (25) $[Cd(\mathbf{L_m})_2]^{2+}$, 371 (22) $[\mathbf{L_m} + H]^+$, 326 (10) $[Cd_2(\mathbf{L_m})_2(OH)]^{3+}$.

Crystallographic Studies. X-ray diffraction intensity data for compounds **1**−**3** were measured on a Bruker SMART APEX CCD-based diffractometer (Mo Kα radiation, λ = 0.710 73 Å).[17] Raw area detector data frame processing was performed with the SAINT+ and SADABS programs.[17] Final unit cell parameters were determined by least-squares refinement of large sets of strong reflections taken from each data set. Direct methods structure solution, difference Fourier calculations, and full-matrix least-squares refinement against F^2 were performed with SHELXTL.[18] Non-hydrogen atoms were refined with anisotropic displacement parameters, the exception being disordered species. The hydrogen atoms were placed in geometrically idealized positions and were included as riding atoms. Details of the data collection are given in Table 1.

Table 1. Selected Crystal Data and Structure Refinement for Complexes 1−3.

	1	2	3
formula	$C_{57}H_{81}Cl_4N_{21}Ni_4O_{26}$	$C_{55.67}H_{83.34}Cl_4N_{20}Ni_4O_{28}$	$C_{52}H_{68}Cl_4Cd_4N_{16}O_{26}$
fw, g mol^{-1}	1853.07	1857.51	1924.62
cryst. syst.	triclinic	monoclinic	monoclinic
space group	$P\bar{1}$	$C2/c$	$P2_1/c$
T, K	150(2)	150(2)	100(2)
a, Å	12.7195(6)	21.7442(12)	13.5923(7)
b, Å	14.3046(7)	17.5713(10)	21.1444(11)
c, Å	21.7466(1)	22.1788(12)	24.2774(12)
α, deg	91.809(1)	90	90
β, deg	93.085(1)	115.890(1)	90.117(1)
γ, deg	106.230(1)	90	90
V, Å^3	3789.1(3)	7623.4(7)	6977.3(6)
Z	2	4	4
$R1$ ($I > 2\sigma(I)$)	0.0569	0.0497	0.0374
w$R2$ ($I > 2\sigma(I)$)	0.1542	0.1314	0.0927

Compound **1** crystallizes in the space group $P\bar{1}$ of the triclinic system. The asymmetric unit consists of one $[Ni_4(\mu_3\text{-}OH)_4(\mu\text{-}\mathbf{L_m})_2(DMF)_4]^{4+}$ cation, four independent perchlorate anions, and one DMF and one ethanol molecule of crystallization. Two of the coordinated DMF molecules (associated with O5 and O8) are disordered over two orientations. These species were refined with the aid of a "same geometry" restraint (SHELX SAME instruction), which restrained their geometries to be similar to that of the well-behaved DMF (O7, N7, C74−C76). The atoms of the disordered DMF molecules and both guest solvent species were refined with isotropic displacement parameters. The electron density map in the vicinity of the noncoordinated DMF and EtOH molecules suggest additional orientations of these species; however, no sensible disorder model could be obtained; the reported coordinates reflect only the major orientation of each of these species. The four bridging hydroxyl hydrogens were located in difference maps and refined isotropically with their O−H distances restrained to be approximately equal. The ethanolic hydrogen could not be located and was not calculated.

Compound **2** crystallizes in the space group $C2/c$. The asymmetric unit consists of half of one $\{Ni_4(\mu_3\text{-}OH)_4(\mu\text{-}\mathbf{L_m})_2(DMF)_2[(H_2O)_{0.79}(MeOH)_{0.21}]_2\}^{4+}$ cation located on a 2-fold axis of rotation, two perchlorate anions, one noncoordinated DMF molecule, and an interstitial region of disordered electron density, which was modeled as a mixture of diethyl ether and methanol. The structure is afflicted with pervasive disorder. The DMF molecule coordinated to Ni2 is disordered over two closely separated, equally populated positions. Interpretation of the electron density map around Ni1 was not straightforward, but eventually this coordination site was modeled as a disordered mixture of 79% water and 21% methanol. Reasonable positions for the water hydrogens were located in a difference map. These were included with d(O−H) = 0.85(2) Å and d(H···H) = 1.40(2) Å distance restraints and U(iso,H) = 1.5U(eq,O). The total population of this site was constrained to sum to unity. The methanolic hydrogen was not located or calculated. Perchlorate Cl1 is disordered and was modeled with two orientations; perchlorate Cl2 shows some elongated displacement ellipsoids but was acceptably modeled with only one orientation. The interstitial region modeled as MeOH/Et_2O is severely disordered, and the model employed should be regarded as approximate. The occupation factors were tied to those of the water/MeOH molecules bonded to Ni1, such that water molecule O3A and MeOH molecule O1S are present together in a given asymmetric unit, and coordinated MeOH O3B and Et_2O molecule O2S are present together. The two independent hydroxyl hydrogens H1A and H2A were located and refined isotropically with d(O−H) = 0.85(2) Å distance restraints. The largest residual electron density peaks are in the vicinity of the disordered methanol/ether molecules, indicating the limitations of the model used.

Crystals of **3** formed as colorless irregular twinned masses. X-ray intensity data were measured from a cleaved fragment. The crystals decompose in air on a time scale of hours. Compound **3** crystallizes in the space group $P2_1/c$. The asymmetric unit consists of one $[Cd_4(\mu_3\text{-}OH)_4(\mu\text{-}\mathbf{L_m})_2(H_2O)_2(acetone)_2]^{4+}$ cation, four perchlorate anions, and two acetone molecules of crystallization. Two perchlorate anions (Cl3 and Cl4) are disordered and were modeled with two closely spaced positions having occupancies Cl3A/Cl3B = 0.53(2)/0.47(2) and Cl4A/Cl4B = 0.779(7)/0.221(7). Total site occupancy was constrained to sum to unity. Geometries of each disorder component were restrained to be similar to that of the ordered perchlorate Cl1. The hydroxyl and water hydrogen atoms were located in difference maps and refined isotropically with a d(O−H) = 0.85(2) Å distance restraint.

RESULTS

Syntheses. Noncrystalline samples were prepared through the reactions of separate methanolic solutions of $\mathbf{L_m}$ and $M(ClO_4)_2{\cdot}6H_2O$, M = Ni(II), Cd(II), Scheme 2. These products contain $[M_4(\mu_3\text{-}OH)_4(\mu\text{-}\mathbf{L_m})_2]^{4+}$ units according to positive-ion electrospray (ESI^+)-MS spectra of the nickel(II) compound and ^1H NMR spectra of the cadmium(II) compound. As we initially anticipated the formation of $[M_2(\mu\text{-}OH)(\mu\text{-}\mathbf{L_m})_2](ClO_4)_3$ type complexes, analogous to those observed with other transition metals,[10] these reactions were carried out with equimolar amounts of ligand and metal salts. Crystals of compound **1**, $[Ni_4(\mu_3\text{-}OH)_4(\mu\text{-}\mathbf{L_m})_2(DMF)_4](ClO_4)_4{\cdot}DMF{\cdot}EtOH$, were isolated by layering EtOH and ether on top of a DMF solution of the initial green powder. The use of MeOH instead of EtOH resulted in crystals of **2**, $\{Ni_4(\mu_3\text{-}OH)_4(\mu\text{-}\mathbf{L_m})_2(DMF)_2[(H_2O)_{0.79}(MeOH)_{0.21}]_2\}(ClO_4)_4{\cdot}2(DMF){\cdot}2[(MeOH)_{0.79}(Et_2O)_{0.21}]$. Crystals of compound **3**, $[Cd_4(\mu_3\text{-}OH)_4(\mu\text{-}\mathbf{L_m})_2(acetone)_2(H_2O)_2](ClO_4)_4{\cdot}2acetone$, were isolated upon vapor diffusion of diethyl ether into a diluted acetone solution of the initial white powder at 5 °C.

Mass Spectrometry. The ESI^+-MS spectra of the nickel(II) and cadmium(II) complexes are similar. Clusters, such as $[M_4(OH)_4(\mathbf{L_m})_2(ClO_4)_3]^+$ and $[M_4(OH)_4(\mathbf{L_m})_2(ClO_4)_2]^{2+}$ are observed for both compounds. In the spectrum of **1**, the base peak is $[Ni_4(OH)_4(\mathbf{L_m})_2(ClO_4)_2]^{2+}$, and even $[Ni_4(OH)_4(\mathbf{L_m})_2(ClO_4)]^{3+}$ could be identified. The base peak for **3** is $[Cd(\mathbf{L_m})(ClO_4)]^+$. Peaks corresponding to clusters containing the coordinated solvent molecules are not observed in the spectra.

Solid-State Structures. Figure 1 presents the cationic unit of **1**, the numbering scheme is correct for both **1** and **3**. Figure 2 shows the cationic unit of compound **2**, which resides on a 2-

dx.doi.org/10.1021/ic403013d | Inorg. Chem. 2014, 53, 4325−4339

Scheme 2. Synthesis of Complexes 1−3

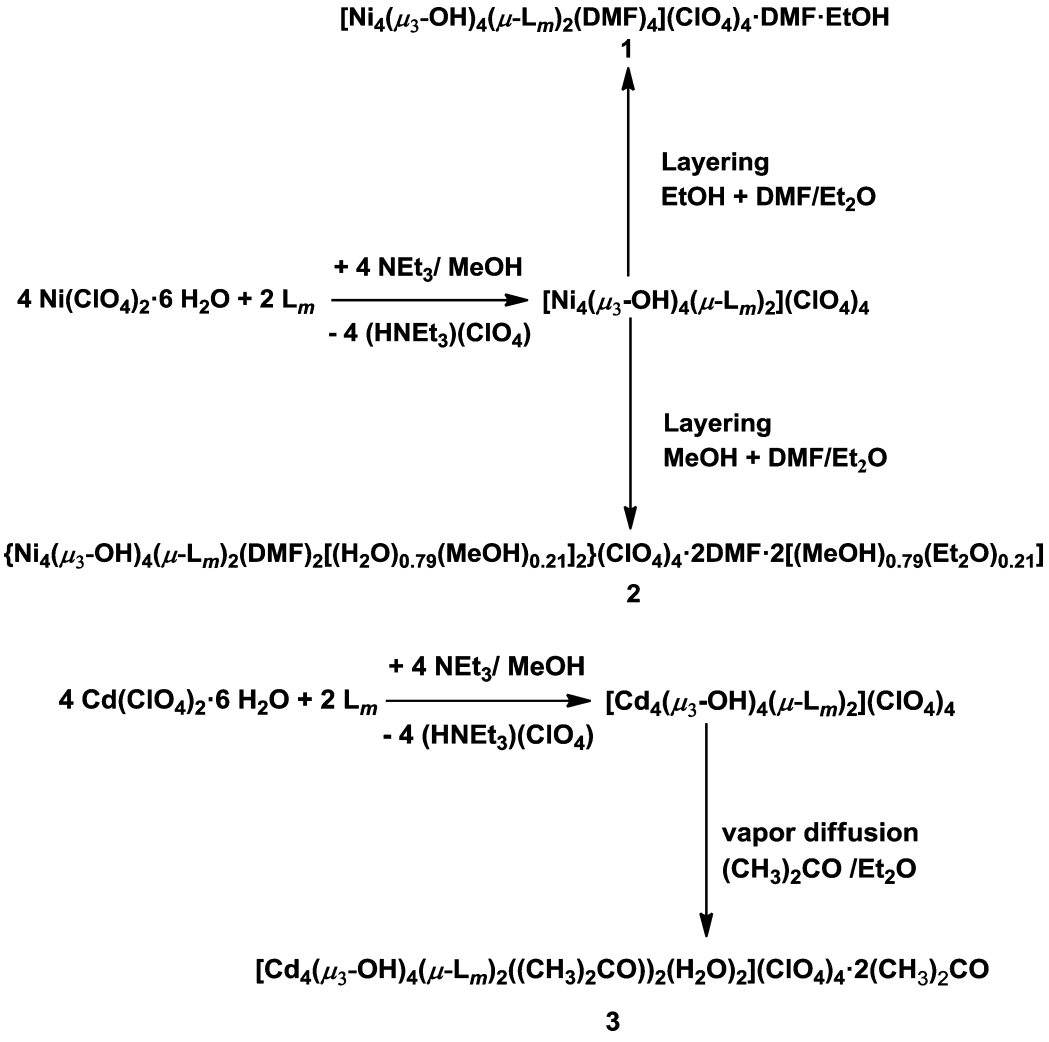

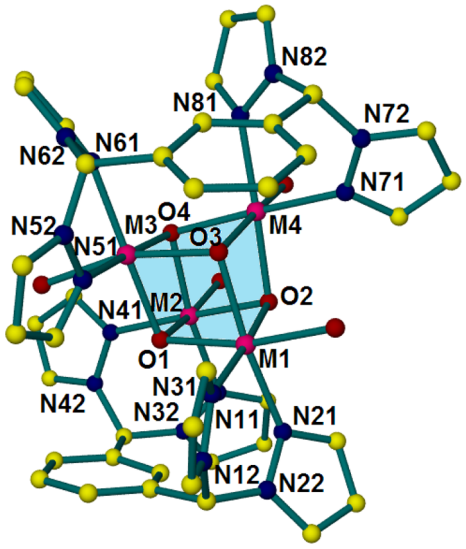

Figure 1. Structure of cationic unit in $[Ni_4(\mu_3\text{-}OH)_4(\mu\text{-}L_m)_2(DMF)_4]\text{-}(ClO_4)_4\cdot DMF\cdot EtOH$, **1**. Hydrogen atoms are omitted for clarity. For the DMF molecules only the oxygen atoms are shown.

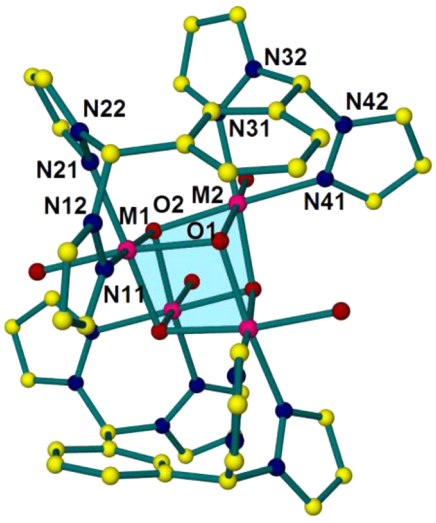

Figure 2. Structure of the cationic unit in $\{Ni_4(\mu_3\text{-}OH)_4(\mu\text{-}L_m)_2(DMF)_2[(H_2O)_{0.79}(MeOH)_{0.21}]_2\}(ClO_4)_4\cdot 2(DMF)\cdot 2\text{-}[(MeOH)_{0.79}(Et_2O)_{0.21}]$, **2**. Hydrogen atoms are omitted for clarity. For the coordinated solvent molecules only the oxygen atoms are shown.

fold axis of rotation. Selected bond lengths and bond angles are shown in Table 2.

dx.doi.org/10.1021/ic403013d | Inorg. Chem. 2014, 53, 4325−4339

Table 2. Selected Bond Lengths and Bond Angles for $[Ni_4(\mu_3\text{-}OH)_4(\mu\text{-}L_m)_2(DMF)_4](ClO_4)_4\cdot DMF\cdot EtOH$ (1), $\{Ni_4(\mu_3\text{-}OH)_4(\mu\text{-}L_m)_2(DMF)_2[(H_2O)_{0.79}(MeOH)_{0.21}]_2\}(ClO_4)_4\cdot 2(DMF)\cdot 2[(MeOH)_{0.79}(Et_2O)_{0.21}]$ (2), and $[Cd_4(\mu_3\text{-}OH)_4(\mu\text{-}L_m)_2(acetone)_2(H_2O)_2](ClO_4)_4\cdot 2$ acetone (3)

complex	T (K)	metal centers	O−M−O angle interval (deg)	average[a] M−O−M angle (deg)	M−O distance interval (Å)	predicted M−O distance, (Å)[b]	average M−N distance (Å)	M···M distance interval (Å)
1	150	Ni(1)	77.91−80.41		2.049−2.063	1.97	2.105	3.122−3.171
		Ni(2)	79.22−80.61	98.69	2.050−2.076		2.116	3.122−3.166
		Ni(3)	77.96−80.22	100.66	2.039−2.069		2.118	3.128−3.171
		Ni(4)	78.85−80.56		2.062−2.072		2.119	3.128−3.167
2	150	Ni(1)	77.73−80.73	98.16	2.056−2.060	1.97	2.102	3.117−3.180
		Ni(2)	78.45−80.89	101.12	2.067−2.070		2.111	
3	100	Cd(1)	77.28−80.82	98.58	2.251−2.284	2.21	2.336	3.458−3.503
		Cd(2)	78.24−80.82		2.265−2.303		2.348	3.454−3.473
		Cd(3)	77.91−80.45	100.98	2.231−2.272		2.323	3.442−3.503
		Cd(4)	78.90−80.95		2.263−2.291		2.375	3.442−3.478

[a]Each value is the average of either six smaller or six larger angles. [b]Shannon Radii, reference 19.

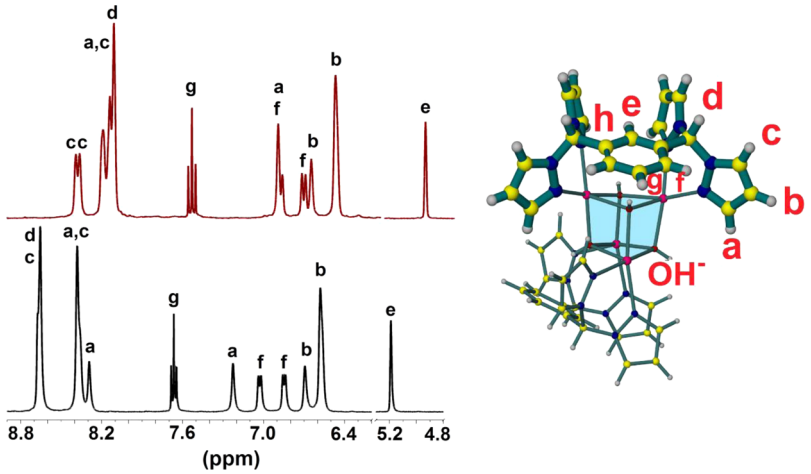

Figure 3. ^{1}H NMR spectra of **3** in acetonitrile (top) and acetone (bottom), the two resonances of the OH^- groups are omitted for clarity. The labeling scheme for the hydrogens is shown on the right: *a*, *b*, *c*—pyrazolyl hydrogens, *d*—methine hydrogen, *e*, *f*, *g*—phenylene hydrogens, *h*—ipso carbon.

In all structures, the geometry around the metal centers is distorted octahedral. The coordination sites of the metal centers are occupied by three hydroxides, two nitrogen atoms from one of the two bis(pyrazolyl)units of the ligand $\mathbf{L_m}$, and one oxygen atom from a coordinated solvent molecule. The bond angles are distorted, with adjacent N−M−N bond angles around 84.83−94.95°, N−M−O angles around 78.85−99.75°, and O−M−O angles around 77.24−80.82°.

Four octahedral metal centers alternating with four triply bridged hydroxide groups at the eight corners of a cube generate a cubane core. The ligand $\mathbf{L_m}$ adopts syn conformation, with both bis(pyrazolyl)methane units on the same side of the phenylene linker. Each $\mathbf{L_m}$ ligand supports the arrangement of the cubane core by connecting two metal ions. The octahedral coordination sphere in the solid state is completed by coordination of a solvent molecule (DMF, MeOH, H_2O, or acetone). These solvent molecules form longer Ni−O (2.092−2.115 Å) and Cd−O (2.325−2.440 Å) bonds than the bridging hydroxide groups (Ni−O 2.039−2.076 Å, Cd−O 2.231−2.291 Å) and are also longer than predicted by the sum of the ionic radii.[19]

The values for the M−O(*H*) distances are larger than predicted by summing the ionic radii of the corresponding metal centers and hydroxide by 0.04−0.08 Å, but are similar to the ones measured in other cubane compounds.[5] Two of the four triply bridging hydroxide groups are oriented toward the phenylene linker forming weak O−H···π interactions [*d*(H··· centroid) = 2.31−2.74 Å, O−H···centroid 143.32−167.85°].[20]

NMR of Cadmium Complex. The cadmium(II) compound was characterized in acetonitrile and acetone solutions. The samples used were dried under vacuum, which results in the loss of coordinated and uncoordinated solvent, resulting in $[Cd_4(\mu_3\text{-}OH)_4(\mu\text{-}L_m)_2](ClO_4)_4$, as shown by the analytical figures. In addition, in the ^{1}H spectra recorded in acetonitrile no acetone is observed. The slightly different spectra in the two solvents helped the identification of several resonances that have very similar chemical shifts and are superimposed in one or the other solvent, Figure 3.

The ambient-temperature ^{1}H and ^{13}C NMR spectra of **3** are complicated, and the resonances are broader than anticipated. To fully interpret these spectra, we recorded the ^{1}H−^{13}C heteronuclear single quantum coherence (HSQC), the ^{1}H−^{13}C heteronuclear multiple bond correlation (HMBC), and the ^{1}H−^{1}H correlation (COSY) spectra of **3** in acetone and acetonitrile (Figure 4) and carried out variable-temperature (VT) studies.

In the ^{1}H NMR spectra of compound **3**, a single resonance can be observed for both the *g* (acetonitrile-d_3 7.56 ppm; acetone-d_6 7.67 ppm) and *e* (acetonitrile-d_3 5.01 ppm; acetone-d_6 5.19 ppm) positions of the phenylene linker, but there are

dx.doi.org/10.1021/ic403013d | Inorg. Chem. 2014, 53, 4325−4339

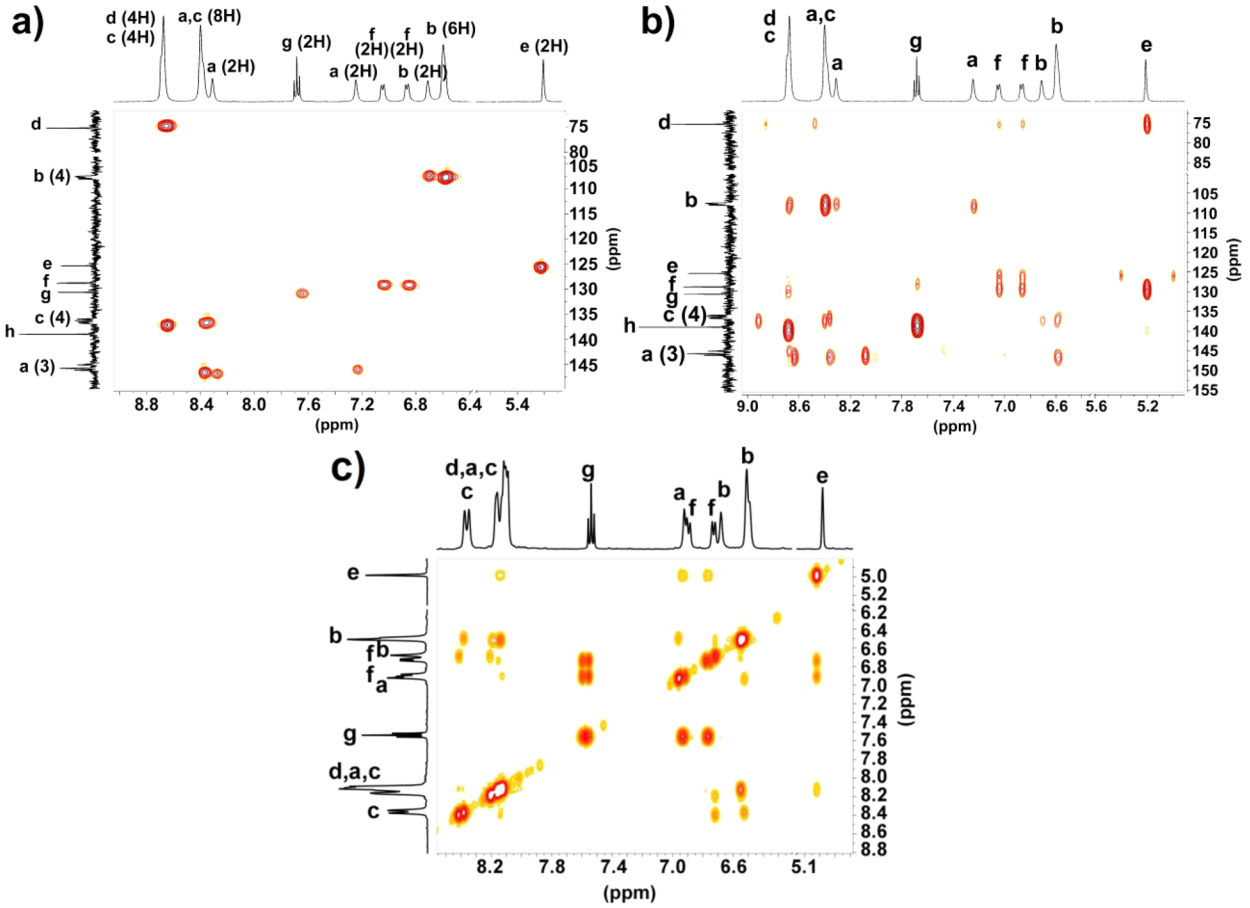

Figure 4. 2D NMR experiments of **3**: HSQC spectrum in acetone-d_6, (a) HMBC spectrum in acetone-d_6, and (b) COSY in acetonitrile-d_3 (c).

two distinct doublets observed for the *f* position (acetonitrile-d_3 6.91 and 6.76 ppm; acetone-d_6 7.02 and 6.84 ppm). In contrast, metallacyclic compounds of the type $[M_2(\mu\text{-F})(\mu\text{-}\mathbf{L_m})_2](BF_4)_3$ (M = Zn(II) or Cd(II))[9a,21] and $[Zn_2(\mu\text{-OH})(\mu\text{-}\mathbf{L_m})_2](ClO_4)_3$[10] show only one set of three resonances for the two phenylene linkers: *e*, *f*, and *g* hydrogens. Although the ^{13}C NMR spectrum of **3** shows one resonance for each of the *e*, *f*, and *g* carbons, the single carbon *f* resonance in acetone is clearly correlated with the two distinct resonances assigned to the *f* hydrogens in the HSQC and HMBC experiments (Figure 4a,b shows the ^{13}C NMR spectra on the Y axes of the two-dimensional (2D) NMR experiments), and two *f* resonances are observed in acetonitrile.

The ^{13}C NMR resonances for the pyrazolyl rings (*a*, *b*, and *c*) of **3** indicate four nonequivalent rings out of a total of eight, as opposed to the previously reported dinuclear species $[Zn_2(\mu\text{-OH})(\mu\text{-}\mathbf{L_m})_2](ClO_4)_3$,[10] where only two distinct environments were observed. The ^{13}C NMR spectrum of **3** in acetone show three signals for the *c*-pyrazolyl carbons (146.1, 145.7, 145.0 ppm) and four signals for both the *a*- (136.8, 136.6, 136.2, 135.8 ppm) and *b*- (108.1, 107.9, 107.7, 107.6 ppm) pyrazolyl carbons. This differentiation cannot be clearly observed in the ^1H NMR spectrum, indicating that some of the pyrazolyl resonances are superimposed. The *b*-pyrazolyl resonances (acetonitrile-d_3 6.70 (2H)/6.52 (6H) ppm; acetone-d_6 6.69 (2H)/6.58 (6H) ppm) integrate to a ratio of 1:3, consistent with four types of pyrazolyl rings in the solution structure.

Another interesting feature in the ^1H NMR spectrum is that one of the *a*- or *c*-position pyrazolyl resonances is unusually shielded (6.94 ppm in acetonitrile-d_3 and 7.23 ppm in acetone-d_6) when compared to the other *a*- and *c*-pyrazolyl resonances (8.40−8.13 ppm in acetonitrile-d_3 and 8.65−8.29 ppm in acetone-d_6). This shielded resonance can be assigned to an *a*-pyrazolyl hydrogen because in the solid-state structure two *a* hydrogens are pointing toward the phenylene linkers and adjacent pyrazolyl ring (H···phenylene(centroid) = 3.44 Å, H···pz(centroid) = 3.28 Å) and are shielded by the π-aromatic electrons (Figure 5), an effect noted previously with $[Zn_2(\mu\text{-OH})(\mu\text{-}\mathbf{L_m})_2](ClO_4)_3$.[10] This assignment makes the *a*- and *c*-

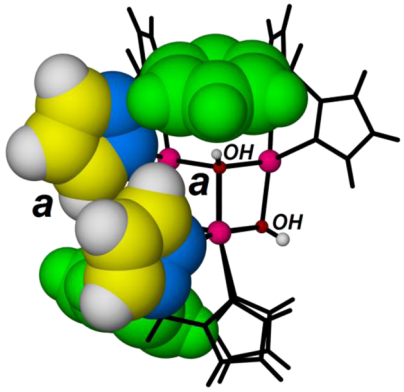

Figure 5. Two *a*-pyrazolyl hydrogens point toward the π-electron clouds of the phenylene and pyrazolyl groups, and one of the two visible triply bridging hydroxides point toward the π-electron cloud of the phenylene linkers. Phenylene linkers are shown in green.

dx.doi.org/10.1021/ic403013d | *Inorg. Chem.* 2014, 53, 4325−4339

positions distinguishable by ^{1}H NMR spectroscopy (Figure 4), when coupled with the VT data (vide infra).

The HSQC and HMBC spectra (Figure 4a,b) show that in acetone at 8.65 ppm the methine resonances are superimposed with two *c*-pyrazolyl hydrogen resonances, and similarly at 8.38 ppm the remaining two *c*-pyrazolyl hydrogen resonances are superimposed with two *a*-pyrazolyl hydrogen resonances. The integrals of these signals are in conformity with these assignments. The remaining *a*-pyrazolyl hydrogen resonances can be observed at 8.29 ppm and at 7.23 ppm, each corresponding to two hydrogens. On the basis of the COSY spectra (Figure 4c) and the assignments above, the spectra of **3** in acetonitrile can be interpreted: the resonances at 8.39 ppm can be assigned to four *c*-pyrazolyl hydrogens, the complicated multiplet centered at 8.16 ppm corresponds to 14 hydrogens: four methine, four *c*-pyrazolyl, and six *a*-pyrazolyl hydrogens, while the multiplet at 6.91 ppm is the signal of the remaining two *a*-pyrazolyl hydrogens superimposed with the signal of one set (two hydrogens) of *f*-phenylene resonances.

The ^{1}H NMR resonances at −2.11 ppm in acetonitrile and at −1.50 ppm in acetone correspond to two bridging OH^- hydrogens,[10,22] also shielded by the π-electron cloud of the phenylene linker (Figure 5). In acetonitrile-d_3 another resonance, also integrating for two hydrogens, can be observed at 2.6 ppm, most clearly at lower temperatures (Figure 7, vide infra). We assign this resonance to the other two bridging hydroxide groups, which are not located below the phenylene linkers. Similarly, the proton-decoupled ^{113}Cd NMR spectrum of **3** shows two distinct cadmium resonances at 3.1 and 1.7 ppm (Figure 6).

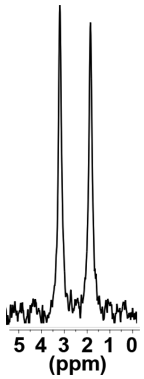

Figure 6. Proton-decoupled ^{113}Cd NMR spectrum of $[Cd_4(\mu_3\text{-}OH)_4(\mu\text{-}L_m)_2(acetone)_2(H_2O)_2](ClO_4)_4$, **3**.

All of these NMR data demonstrate that the solid-state cubane-core structure is retained in solution. Given the weakly coordinated solvents observed in the solid-state structures, the coordinating NMR solvents may be rapidly exchanging on the NMR time scale, but this exchange would not impact the assignments of the spectra. Therefore, one expects four types of pyrazolyl rings and two types of "cubane" positions for the hydroxide (one set of hydrogens pointing toward the phenylene linker (O1) and the other at the back side of this bridging ligand (O2)) and cadmium vertices, a structure similar to that shown in Figure 2 for nickel(II) with the coordinated solvent removed (drawing in Figure 3). Two hydroxide groups and cadmium(II) cations, together with the pyrazolyl rings of each $\mathbf{L_m}$ ligand are symmetry-related by the 2-fold rotation axis passing through the middle of the cubane core, similar to that observed for the solid-state structure of compound **2**.

Results of the diffusion experiment, pulsed field-gradient spin echo (PGSE), also support the presence of the tetrameric form in solution. The hydrodynamic radius of **3** in acetonitrile, calculated based on the diffusion coefficient measured by PGSE NMR, was determined as 8.4 Å. This number agrees with the maximum radius (also 8.4 Å) calculated from the X-ray structure for a hypothetical sphere generated around the cubane compound.

Variable-Temperature ^{1}H NMR. As observed previously with $[Zn_2(\mu\text{-}OH)(\mu\text{-}L_m)_2](ClO_4)_3$, a molecule that we have shown to display a very unusual fluxional process,[10] the pyrazolyl hydrogen resonances of **3** are broad at room temperature. Upon increasing the temperature of **3** in acetonitrile-d_3, the pyrazolyl resonances broaden substantially and start to equilibrate, indicating that this molecule is also fluxional.[23] To study this process, we recorded the variable-temperature ^{1}H NMR (VT NMR) spectra of **3** over the liquid range of acetonitrile-d_3, as shown in Figure 7.

Even though the temperature range accessible in acetonitrile-d_3 is relatively narrow (−40 to 75 °C) and the limiting high-temperature spectra could not be reached, the data indicate that the four resonances for each type of pyrazolyl hydrogen, the

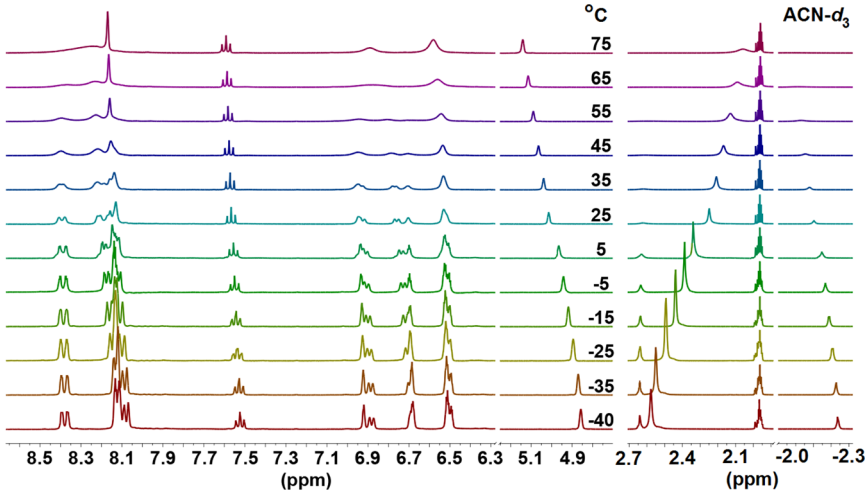

Figure 7. The VT ^{1}H NMR spectra of complex **3** over the liquid range of acetonitrile-d_3.

dx.doi.org/10.1021/ic403013d | *Inorg. Chem.* 2014, 53, 4325−4339

two *f*-position resonances and the two hydroxide resonances observed at lower temperatures, coalesce at higher temperatures. The rate constant for the pyrazolyl exchange (k_{Lm}) was modeled successfully by simulation of the *c*-pyrazolyl resonance line widths using DNMR as implemented in Spinworks.[24] We chose to simulate the line widths of the *c*-pyrazolyl resonance because that set was most clearly separated from other resonances. The Gibbs energy of activation $\Delta G^{\ddagger}_{Lm}$, enthalpy of activation $\Delta H^{\ddagger}_{Lm}$, and entropy of activation $\Delta S^{\ddagger}_{Lm}$ were calculated based on the Eyring plot (Figure 8). The $\Delta H^{\ddagger}_{Lm}$

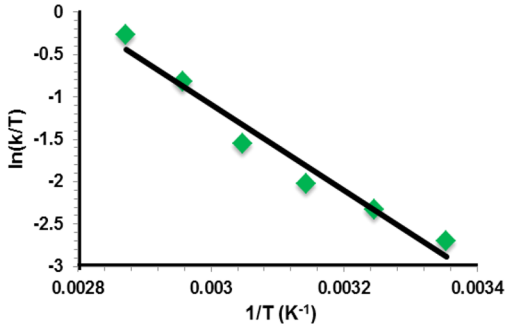

Figure 8. Eyring plot based on simulated k_{Lm} values for **3**, where slope = $-\Delta H^{\ddagger}_{Lm}/R$; intercept = $\Delta S^{\ddagger}_{Lm}/R$ + 23.7600. Green squares: experimental data, Black line: least-squares fit, R^2 = 0.96.

based on the Eyring plot is 10.1 ± 0.5 kcal/mol, while the $\Delta S^{\ddagger}_{Lm}$ is −19.2 ± 1.0 cal/mol K. The Gibbs energy of activation was calculated based on the fundamental equation: $\Delta G^{\ddagger}_{Lm} = \Delta H_{Lm}{}^{\ddagger} - T \times \Delta S^{\ddagger}_{Lm}$ and gave $\Delta G^{\ddagger}_{Lm}$ = 15.8 ± 0.8 kcal/mol at 25 °C.

For the VT NMR experiment a different sample was used than for the room-temperature NMR studies, which resulted in different trace amounts of water in the sample (from acetonitrile-d_3). The shapes of the pyrazolyl resonances (at the same temperature) were affected by this change in the water concentration, and as a consequence the magnitude of the rate constant changed. Since the absolute concentration of the water is unknown, we expressed it as the ratio of the integral of water divided by the integral of the *e*-position of the ligand signal at 25 °C. The relative water concentration in the sample used for room-temperature NMR studies is 1.8, and in the sample used for VT NMR experiments it is 2.3. At the same temperature, the pyrazolyl resonances in the sample with more water (2.3) are broader than the same resonances in the sample with less water (1.8), indicating that the rate of the pyrazolyl exchange increases at higher concentrations of water. The line widths of the *f*-resonances also change, but the *g*- and *e*-resonances are not affected by the change in the water concentration.

Saturation Transfer Experiments. Two different saturation transfer experiments were performed on an acetonitrile-d_3 sample of **3**. The first experiment targeted the exchange process between the nonequivalent *a*-pyrazolyl hydrogens—the same process studied by VT NMR, while in the second experiment we studied the exchange of the trace amount of water with the bridging hydroxide groups.

During these experiments, one of the exchanging resonances is saturated, and the effect on the intensity of the second resonance is monitored. To determine the rate constant for the exchange, we measured the decrease in the intensity of the exchanging resonance as a function of increased saturation times at the site of the other exchanging resonance. The saturation time was increased by 0.25 s until the intensity of the resonance remained constant. The plot of the values of $\ln[I_i - I_\infty]$ (I_i = residual intensity after intermediate amounts of saturation times, and I_∞ = final intensity) against the saturation time (t) results in a straight line. The slope of this line permits the determination of the rate constant, if the process is first order (see Supporting Information for details).[25]

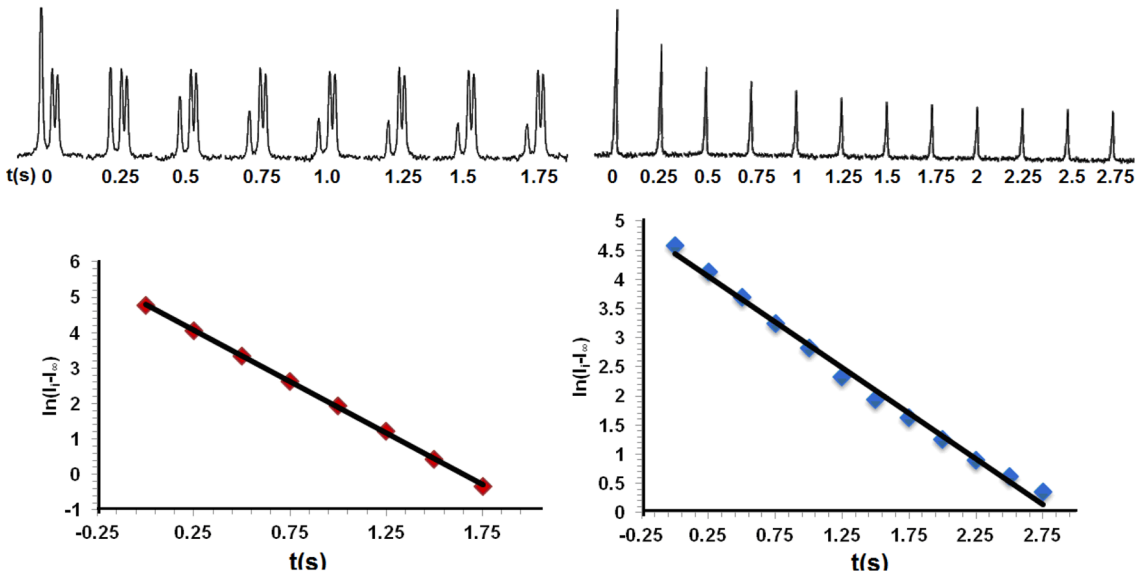

Figure 9. Saturation transfer experiment in acetonitrile-d_3 at 0 °C for **3**. (top left) Decrease of the *a*-pz resonance as a function of saturation time. For the *a*-pyrazolyl exchange the phenylene doublet (*f*) was included in the figure. As the intensity of the pyrazolyl resonance decreases upon increased saturation times, the intensity of the doublet is constant, since the *f* hydrogens are not exchanging with the other *a*-pz hydrogens. (bottom left) Linear plot of the saturation time vs the natural logarithm of the *a*-pz resonance intensities. (top right) Decrease of the OH^- resonance as a function of saturation time. (bottom right) Linear plot of the saturation time vs the natural logarithm of the OH^- resonance intensities. Red and blue squares: experimental data; black line: least-squares fit, R^2 = 0.99.

dx.doi.org/10.1021/ic403013d | Inorg. Chem. 2014, 53, 4325−4339

In the first experiment, the overlapping *a*-pyrazolyl hydrogen resonances (~8.16 ppm) were saturated, while we monitored the effect of this saturation on the shielded *a*-pyrazolyl resonance (6.94 ppm). Since in this case the extra chemical shift difference between the two exchanging *a*-pyrazolyl resonances is an advantage, the *a*-pyrazolyl resonances were used for the experiment, instead of the *c* resonances used for the VT NMR. To avoid cross saturation of the pyrazolyl resonances the sample was cooled to 0 °C. Data collected during the saturation transfer experiment is shown in Figure 9, left.

In the second experiment the water hydrogen resonance (~2.35 ppm) was saturated. We monitored the decrease in the intensity of the shielded bridging OH^- hydrogen resonance (−2.15 ppm) as a function of increased saturation times (Figure 9, right).

At 0 °C, for the *a*-pyrazolyl exchange the calculated k_{Lm} is 2.18 ± 0.1 s^{-1} and $\Delta G^{\ddagger}_{Lm}$ is 15.5 ± 0.3 kcal/mol. For the water−hydroxide exchange the k_{OH} is 1.16 ± 0.1 s^{-1} and the $\Delta G^{\ddagger}_{OH}$ is 15.9 ± 0.3 kcal/mol. The rate constants and activation barriers calculated for the pyrazolyl exchange from the saturation transfer measurements are in very good agreement with the analogous value calculated from VT NMR experiments ($\Delta G^{\ddagger}_{Lm}$ = 15.3 ± 0.8 kcal/mol at 0 °C for the same sample).

Magnetic Properties of $[Ni_4(\mu_3\text{-}OH)_4(\mu\text{-}L_m)_2(DMF)_4](ClO_4)_4\cdot DMF\cdot EtOH$, 1. The effective magnetic moment, calculated per entire tetranuclear molecule, is 6.53 μ_B at 300 K, somewhat higher than that expected for four noninteracting nickel(II) ions with a *g* value of about 2.2 ($\mu_{eff} = g(4S(S+1))^{1/2}$ = 6.22). Upon lowering the temperature, μ_{eff} increases to reach a maximum of 9.75 μ_B at 5.5 K and then decreases to 8.74 at 1.8 K (Figure 10). The maximum μ_{eff} value is close to that expected

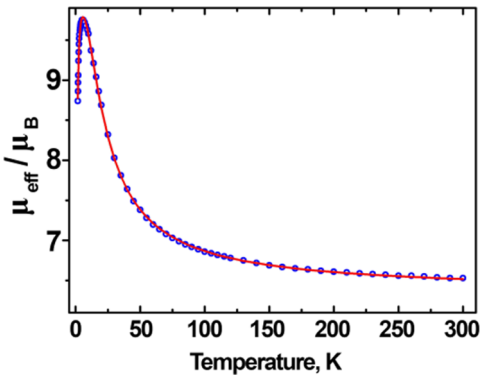

Figure 10. The experimental effective magnetic moments (circles) and calculated (solid line) referred to four nickel(II) ions. The fitting procedure (eq 4) resulted in g_{ave} = 2.24, D_i = 5.8 cm^{-1}, E_i = 2.3 cm^{-1} (*g*, D_i, and E_i assumed to be the same for all four metal ions, but their orientations in space are different), J_1 = 9.1 cm^{-1}, J_2 = 2.1 cm^{-1}.

for a tetranuclear nickel(II) system with only the S = 4 state populated ($\mu_{eff} = g(S(S+1))^{1/2}$ = 9.84). This behavior indicates weak ferromagnetic interactions between the nickel ions. The magnetic moment decrease at the lowest temperatures is caused by the Zeeman splitting plus the zero-field splitting (zfs) becoming comparable to the thermal energy kT. The structure of the molecular core (Figure 1) reveals that each nickel(II) ion is connected to its three neighbors by three oxygen atoms. If the Ni_4 core had tetrahedral symmetry then all six exchange coupling constants J_{ij} would be equal. However, upon closer examination, two types of Ni−O−Ni angles can be distinguished (Table S1 in the Supporting Information): in the first group, the Ni−O−Ni angles are in the range from 97.9 to 99.5° (Ni1−Ni2, Ni2−Ni4, and Ni3−Ni4), while the angles are slightly larger in the second group, from 100.3 to 101.5° (Ni1−Ni3, Ni1−Ni4, and Ni2−Ni3). One may thus expect two kinds of exchange interactions, the one in the first group being more ferromagnetic. It should be emphasized that this is an approximation to obtain a manageable model, while in fact all six exchange coupling constants are likely to be different. The Heisenberg−Dirac−Van Vleck (HDVV) Hamiltonian for the isotropic exchange interactions will have the form

$$\hat{\mathbf{H}}_{HDVV} = -J_1(\hat{\mathbf{S}}_1\hat{\mathbf{S}}_2 + \hat{\mathbf{S}}_2\hat{\mathbf{S}}_4 + \hat{\mathbf{S}}_3\hat{\mathbf{S}}_4) - J_2(\hat{\mathbf{S}}_1\hat{\mathbf{S}}_3 + \hat{\mathbf{S}}_1\hat{\mathbf{S}}_4 + \hat{\mathbf{S}}_2\hat{\mathbf{S}}_3) \quad (1)$$

The total spin of our tetranuclear system is defined as

$$\hat{\mathbf{S}}_T = \hat{\mathbf{S}}_1 + \hat{\mathbf{S}}_2 + \hat{\mathbf{S}}_3 + \hat{\mathbf{S}}_4 \quad (2)$$

Exchange interactions result in one S_T = 4 state, three S_T = 3 states, six S_T = 2 states, six S_T = 1 states, and three S_T = 0 states. If $J_1 = J_2$ in eq 1 then all states with a given S_T have the same energy, but are split otherwise.

Non-negligible zfs effects are also expected. In polynuclear transition metal systems there are three sources of zfs: the magnetic dipole−dipole interactions, the anisotropic exchange interactions, and the zfs on individual ions, if their spin is larger than 1/2. The third contribution should be the most important in our case, as nickel(II) is known to exhibit large D and E parameters[26] corresponding to the spin Hamiltonian

$$\hat{\mathbf{H}}_i^{zfs} = D_i[\hat{\mathbf{S}}_{zi}^{\,2} - S_i(S_i+1)/3] + E_i(\hat{\mathbf{S}}_{xi}^{\,2} - \hat{\mathbf{S}}_{yi}^{\,2}) \quad (3)$$

where the index i = 1 to 4 [nickel(II) ions]. A full spin Hamiltonian to describe the magnetic properties as well as the electron paramagnetic resonance spectra is

$$\hat{\mathbf{H}} = \hat{\mathbf{H}}_{HDVV} + \hat{\mathbf{H}}_1^{zfs} + \hat{\mathbf{H}}_2^{zfs} + \hat{\mathbf{H}}_3^{zfs} + \hat{\mathbf{H}}_4^{zfs} + \mu_B B(\{\mathbf{g}_1\}\hat{\mathbf{S}}_1 + \{\mathbf{g}_2\}\hat{\mathbf{S}}_2 + \{\mathbf{g}_3\}\hat{\mathbf{S}}_3 + \{\mathbf{g}_4\}\hat{\mathbf{S}}_4) \quad (4)$$

The last term represents the Zeeman interaction. The $\{\mathbf{g}_i\}$, D_i, and E_i values will be assumed equal for all four nickel(II) ions, but the $\{\mathbf{g}_i\}$ and zfs tensors of the four nickel(II) ions are not coaxial. The anisotropic exchange contribution will not be considered.

The magnetic field dependence of the magnetization of **1** measured at 2.0 K (Figure 11) confirms the S = 4 ground state of the system and can be best reproduced when using the coupled-spin Hamiltonian (eq 5, see next section) with the zfs parameters as found from EPR and slightly increased g_{ave} value (2.24 vs g_{aveEPR} = 2.19).

EPR Spectra of $[Ni_4(\mu_3\text{-}OH)_4(\mu\text{-}L_m)_2(DMF)_4](ClO_4)_4\cdot DMF\cdot EtOH$, 1. Well-resolved spectra coming from the ground S_T = 4 state of the tetranuclear molecule were observed at high microwave frequencies of ca. 50−430 GHz at low temperatures (Figure 12). No resolved spectra of excited spin states could be observed at any temperature. The temperature dependence of the spectra allowed determination of the sign of the zfs parameters D and E, which were found to be negative. The coupled-spin state Hamiltonian (eq 5) with S = 4 was used in the EPR simulations (Figure 13 and Figures S3 and S4 in the Supporting Information):

dx.doi.org/10.1021/ic403013d | Inorg. Chem. 2014, 53, 4325−4339

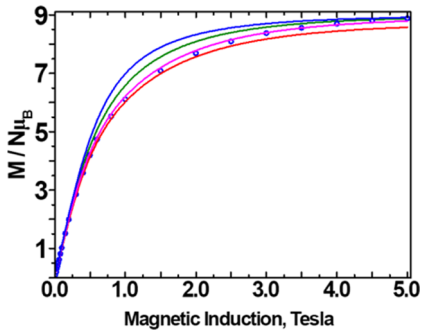

Figure 11. Magnetic field dependence of the magnetization of **1** at 2.0 K. Circles: experimental. Green line: calculated using Hamiltonian (4). Red (bottom): calculated for $S = 4$ using the coupled-spin Hamiltonian (eq 5) with $g_x = 2.205$, $g_y = 2.157$, $g_z = 2.204$, $D = -0.299$ cm^{-1}, $E = -0.036$ cm^{-1}, $B_4^0 = -3.7 \times 10^{-5}$ cm^{-1}, $B_4^2 = 4.2 \times 10^{-4}$ cm^{-1}, and $B_4^4 = -1.6 \times 10^{-4}$ cm^{-1}. Purple: calculated with $g_x = g_y = g_z = g_{ave} = 2.24$ and other parameters as above. Blue (top): calculated using the coupled-spin Hamiltonian with $g_{ave} = 2.24$ and all zfs parameters equal to 0.

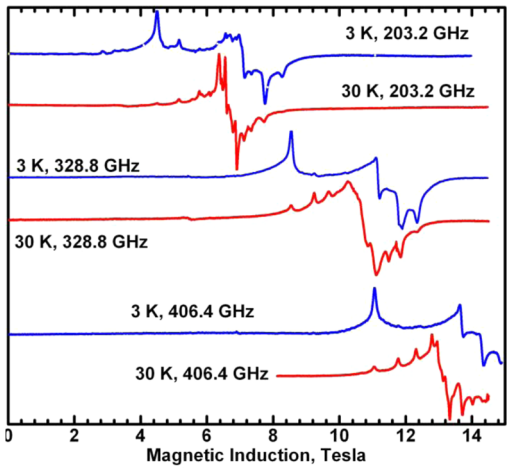

Figure 12. EPR spectra of **1** at temperatures and microwave frequencies as indicated. The intense transition at the low field in the three 3 K spectra is the first (of eight) "allowed" parallel (Z) transitions in the $S = 4$ spin state, occurring between the $M_S = -4$ and $M_S = -3$ states (see Figure S2 in the Supporting Information). The $M_S = -4$ state is the only one significantly populated at 3 K and at high magnetic field. More transitions appear at 30 K as the states $M_S = -3$, -2, etc. become populated. The highest-field feature in the 203.2 and 328.8 GHz spectra is the Y transition. The intensity relations allow the determination of the negative sign of the D parameter in the spin Hamiltonian for $S = 4$.

$$\hat{H}_{S=4} = \mu_B B(\{\mathbf{g}\}\hat{\mathbf{S}} + D[\hat{\mathbf{S}}_z^2 - S(S+1)/3] + E(\hat{\mathbf{S}}_x^2 - \hat{\mathbf{S}}_y^2) + B_4^0 O_4^0 + B_4^2 O_4^2 + B_4^4 O_4^4 \quad (5)$$

The more correct procedure using the spin Hamiltonian in eq 4 is prohibitively difficult with respect to the calculation time, and many needed parameters cannot be predicted, like the orientations of the g and zfs tensors of the four nickel ions. The spin Hamiltonian (eq 5) parameters were found by fitting the positions of the prominent resonances observed in the 30 K spectra measured at many microwave frequencies over the range of 96−432 GHz (Figure S1 in the Supporting Information): $g_x = 2.205$, $g_y = 2.157$, $g_z = 2.204$, $D = -0.299$ cm^{-1}, $E = -0.036$ cm^{-1}, $B_4^0 = -3.7 \times 10^{-5}$ cm^{-1}, $B_4^2 = 4.2 \times 10^{-4}$ cm^{-1}, $B_4^4 = -1.6 \times 10^{-4}$ cm^{-1}.

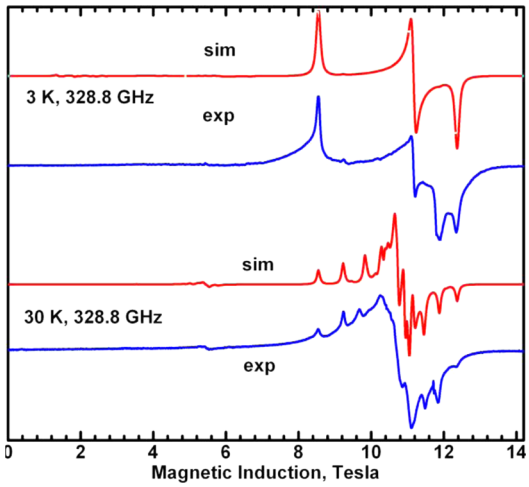

Figure 13. EPR spectra of **1**: Blue: experimental, red: simulated for $S = 4$ with $g_x = 2.205$, $g_y = 2.157$, $g_z = 2.204$, $D = -0.299$ cm^{-1}, $E = -0.036$ cm^{-1}, $B_4^0 = -3.7 \times 10^{-5}$ cm^{-1}, $B_4^2 = 4.2 \times 10^{-4}$ cm^{-1}, $B_4^4 = -1.6 \times 10^{-4}$ cm^{-1}. The broad feature overlapping with the $S = 4$ spectrum at 30 K may be due to the excited spin states. Simulation of a 30 K, 222.4 GHz spectrum is shown in Figure S3 in the Supporting Information.

The necessity of including the fourth-order spin operators in the EPR simulations may be an artifact caused by the mixing of the levels belonging to different S_T states by the zfs and the Zeeman interactions. Similar effects have been observed before.[26,27] The relationships between the zfs parameters D_i and E_i of the single-ion Hamiltonian (eq 3) and the D and E parameters of the "giant spin" Hamiltonian (eq 5) are known.[28] For example, in the case of a nickel(II) tetranuclear compound, in which the zfs tensors on all individual ions are parallel and equal, a D_i value of Hamiltonian, eq 3, would result in $D = D_i/7$ in the spin Hamiltonian, eq 5, for the $S = 4$ state. However, in the present case, the D and E values of the four nickel(II) ions are unlikely to be equal, and moreover, their orientations are impossible to predict. Determining zfs on individual nickel(II) ions from the spin-Hamiltonian parameters found for the coupled $S = 4$ state is therefore impossible. The spin Hamiltonian, eq 5, was successfully used here to simulate the EPR spectra (Figure 13, S3 in the Supporting Information) as well as the field dependence of the magnetization at 2 K (Figure 11). The magnetic-susceptibility temperature dependence was fitted using spin Hamiltonian in eq 4 with two triads of equal J values as explained above (eq 1) and assuming a model in which the zfs tensors of all nickel(II) ions are equal and their Z orientation is chosen along the respective Ni−O_{DMF} directions. These simplifications are unavoidable, as there is no chance of extracting more parameters from the magnetic susceptibility. The fitting (Figure 10) resulted in two significantly different J values $J_1 = 9.1$ cm^{-1} and $J_2 = 2.1$ cm^{-1} (eq 1) and strongly nonaxial zfs parameters for the nickel(II) ions (eq 3, 4). Fitting only the higher temperature data (above 10 K), which are less sensitive to the zfs effects, produced essentially the same J_1 and J_2 values.

Density Functional Theory Calculations for [$Ni_4(\mu_3$-OH)$_4(\mu$-$L_m)_2(DMF)_4$](ClO$_4$)$_4$·DMF·EtOH, 1. "Broken symmetry"[29] density functional theory (DFT) calculations were performed using the software package ORCA[30] to get more insight into the exchange interactions in this system. The X-ray

dx.doi.org/10.1021/ic403013d | Inorg. Chem. 2014, 53, 4325−4339

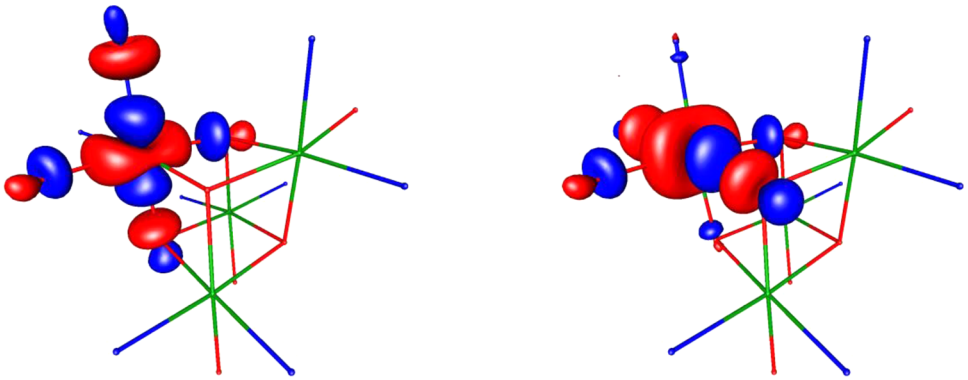

Figure 14. Magnetic orbitals of one of the nickel(II) ions calculated from DFT. Only the metal atoms and the coordinated ligand atoms are shown. Only the metal atoms and the coordinated ligand atoms are shown. Left: the $d_{x^2-y^2}$ type orbital; right: the d_{z^2}-type orbital. Corresponding orbitals of the same shape are located on another nickel(II) ion in an interacting pair. The overlap integrals of the $d_{x^2-y^2}$ type magnetic orbitals are 0.038 and 0.047 for the pairs with smaller Ni−O−Ni angles (around 98−99°) and larger angles (around 100°), respectively. The overlaps of the d_{z^2}-type magnetic orbitals are 0.014 and 0.016, respectively.

coordinates were used in the calculations, but the tetranuclear molecule was simplified by converting DMF into formamide and by removing the benzene rings from the $\mathbf{L_m}$ ligand and putting H atoms at appropriate positions. To calculate J between a pair of nickel(II) ions, the two remaining nickel(II) ions were replaced with zinc(II). The TZVPP function base was used for nickel(II) and all coordinated atoms, while VDZ functions were used for other atoms.[31] The B3LYP functional was employed.[32] In the broken symmetry procedure, a SCF calculation is first performed on a molecule in the high-spin state (HS), which in our simplified Ni_2Zn_2 system is an $S = 2$ state. Next, a broken symmetry state (BS) is set up in which two unpaired electrons on one nickel(II) are spin-up and two electrons on another nickel(II) are spin-down, and a second SCF calculation is performed. The exchange coupling constant is then evaluated using $J = (E_{HS} - E_{BS})/[S_{max}(S_{max} + 1)]$. This equation is applicable for weak exchange interactions according to the ORCA manual. One calculation was performed for the pair in which the Ni−O−Ni angles were larger ($Ni_1O_1Ni_3$ and $Ni_3O_3Ni_1$) and another for a pair with smaller Ni−O−Ni anglesangles (Ni_1O1Ni_2 and $Ni_1O_2Ni_2$). The calculation was indeed able to distinguish between these situations, although the calculated J values were less different from each other than were those found from the magnetic susceptibility. Ferromagnetic interactions were found in each case, which were stronger (12.2 cm^{-1}) for the smaller Ni−O−Ni angle and weaker (6.8 cm^{-1}) for the larger Ni−O−Ni angle, as expected. The calculated J values were overestimated compared to the results of the magnetic susceptibility fitting. The weakening of the ferromagnetic character of the interaction with increasing Ni−O−Ni angles is associated with the increasing overlap of the magnetic orbitals, which favors the antiferromagnetic contribution to the overall metal−metal interaction.[33] There are two magnetic orbitals on each nickel(II) ion, as shown in Figure 14, which also gives the overlap integrals with their counterparts located on another nickel(II) ion. The four single-occupied molecular orbitals of the Ni_2Zn_2 system are shown in Figure S4 in the Supporting Information.

DISCUSSION

We synthesized nickel(II) and cadmium(II) cubane-core compounds where the corners of the "cube" are occupied by four metal centers alternating with four hydroxide bridges. This arrangement is supported by the ditopic bis(pyrazolyl)methane ligand $\mathbf{L_m}$ and additional solvent molecules from the crystallization procedure in the solid state to give compounds of the type $[M_4(\mu_3\text{-}OH)_4(\mu\text{-}\mathbf{L_m})_2(solvent)_4](ClO_4)_4$, with octahedral metal centers. The cubane core is highly stable in the gas phase and solution as indicated by ESI^+-MS and NMR experiments. While several cubane-cored coordination compounds are known, this type of cluster is rarely generated by triply bridging hydroxide groups.[5,6] The formation of these cubane complexes with nickel(II) and cadmium(II) is in contrast with the formation of dinuclear $[M_2(\mu\text{-}OH)(\mu\text{-}\mathbf{L_m})_2](ClO_4)_3$ for M = Fe(II), Co(II), Cu(II), Zn(II) that form under the same reaction conditions.[10] This result parallels somewhat the chemistry of the fluoride-bridged $[M_2(\mu\text{-}F)(\mu\text{-}\mathbf{L_m})_2](BF_4)_3$, M = Fe(II), Co(II), Cu(II), Zn(II), complexes, where analogous synthetic procedures yielded *difluoride*-bridged compounds, $[M_2(\mu\text{-}F)_2(\mu\text{-}\mathbf{L_m})_2](BF_4)_2$ with nickel(II) and cadmium(II).[9]

The cubane core can be seen as being assembled from two bridged dinuclear units of the type $[M_2(\mu\text{-}OH)_2(\mu\text{-}\mathbf{L_m})\text{-}(solvent)_2]^{2+}$. From this view of the cubane compounds, it is straightforward to envisage a C_2 axis of rotation passing through the middle of the cube and bilateral symmetry as observed for compound **2** in the solid state (Figure 15) and for compound **3** in solution.

The cadmium(II) compound was characterized in solution by a series of NMR experiments that support the cubane structure in acetonitrile and acetone solutions. The 2D NMR experiments (HSQC, HMBC, and COSY) facilitated the assignment of the complicated ^1H NMR spectrum (some resonances are accidentally superimposed, isochronous). In these spectra, we observe two nonequivalent sites of cadmium(II) centers and hydroxides, while there are four different types of pyrazolyl rings, and the phenylene linker has two nonequivalent f hydrogens, all in agreement with a cubane core arrangement with a C_2 axis of rotation on average in solution (Figure 15).

The VT ^1H NMR and saturation transfer experiments show that each type of pyrazolyl hydrogen is exchanging, as well as the f positions of the phenylene linkers and hydroxide resonances. The four broad pyrazolyl resonances for each type of ring hydrogen and the two f phenylene resonance and bridging hydroxide resonances broaden and/or coalesce at

dx.doi.org/10.1021/ic403013d | Inorg. Chem. 2014, 53, 4325−4339

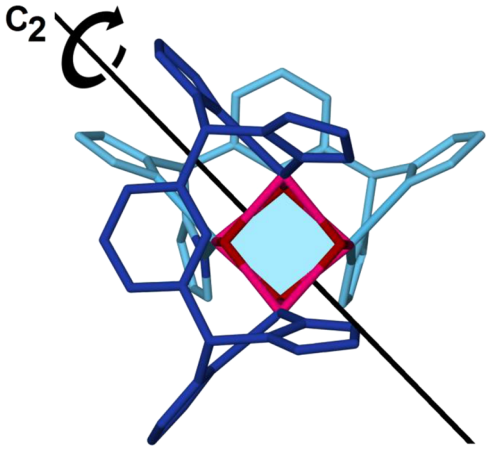

Figure 15. The crystal structure of **2** highlighting the C_2 axis passing through the middle of the cube. Solvents and hydrogen atoms are omitted for clarity of the figure. Color code: $\mathbf{L_m}$ blue, nickel(II) pink, OH^- oxygen red. Darker shades of blue are on the top of the cube, and lighter shades are in the back. The solution structure of the cation $[Cd_4(\mu_3\text{-}OH)_4(\mu\text{-}\mathbf{L_m})_2]^{4+}$ is analogous, making two cadmium(II) centers and the two ligands symmetry equivalent.

higher temperatures. This behavior is somewhat similar to our previous reports on the dinuclear zinc(II) metallacycle $[Zn_2(\mu\text{-}OH)(\mu\text{-}\mathbf{L_m})_2](ClO_4)_3$,[10a] where we showed that the two sets of nonequivalent pyrazolyl rings, axial and equatorial in a trigonal bipyramidal geometry around zinc(II), exchange through a Berry pseudorotation mechanism at *both metal sites* accompanied by the simultaneous 180° ring flip of the phenylene linkers, a rearrangement process we termed the "Columbia Twist and Flip."

Similarly for **3**, we demonstrate above that the cubane core is retained in solution, but the weakly coordinating solvents are lost and/or exchanging rapidly on the NMR time scale, resulting in effectively five-coordinate cadmium(II) centers on average. In this system, three oxygen positions are fixed in the cubane core, while the remaining two positions are occupied by the $\mathbf{L_m}$ pyrazolyl rings. To explain the NMR behavior of **3** presented here, we propose a similar rearrangement process to that previously reported for $[Zn_2(\mu\text{-}OH)(\mu\text{-}\mathbf{L_m})_2](ClO_4)_3$, where pairs of pyrazolyl rings at each of the two metals linked by $\mathbf{L_m}$ twist with the simultaneous 180° flip of the phenylene linker along the $C_{methine}-C_{Ph}$ bond according to Figure 16, the Columbia Twist and Flip mechanism. The twist and flip mechanism of both ligands equilibrates all four nonequivalent pyrazolyl rings. In addition, these motions result in the exchange of the *f* positions of the phenylene linkers, as well as the two nonequivalent cadmium(II) and hydroxide sites. This mechanism is similar to that observed previously with $[Zn_2(\mu\text{-}OH)(\mu\text{-}\mathbf{L_m})_2](ClO_4)_3$ and has the advantage of no bond cleavage, and relatively small bond angle changes are needed around the cadmium(II) ions. The $\Delta G^{\ddagger}_{Lm}$ for the process with **3** is 15.8 kcal/mol at 25 °C, slightly higher than the one measured for $[Zn_2(\mu\text{-}OH)(\mu\text{-}\mathbf{L_m})_2](ClO_4)_3$, which is 15.2 kcal/mol at 25 °C. In addition, both systems show unusually large, negative $\Delta S^{\ddagger}_{Lm}$ values.

We also showed that in both this new tetranuclear system, and the dinuclear system studied previously, the line widths of the exchanging resonances are dependent on the trace water (from acetonitrile-d_3) concentration in the sample; the more water in the sample, the broader the *a*, *b*, and *c*-pyrazolyl and *f*-phenylene resonances become in the room-temperature ^1H NMR spectra. In addition, saturation transfer experiments at 0 °C show that the hydroxide and water hydrogens exchange, with $\Delta G^{\ddagger}_{OH}$ is 15.9 kcal/mol. This process has a slightly higher energy barrier than the pyrazolyl exchange, 15.3 kcal/mol at 0 °C, as was previously observed with $[Zn_2(\mu\text{-}OH)(\mu\text{-}\mathbf{L_m})_2](ClO_4)_3$. Considering the experimental results above, the twist and flip motion of $\mathbf{L_m}$ in the cubane compounds and the water–hydroxide exchange are probably independent but related processes.

For $[Ni_4(\mu_3\text{-}OH)_4(\mu\text{-}\mathbf{L_m})_2(DMF)_4](ClO_4)_4\cdot DMF\cdot EtOH$, **1**, both the magnetic susceptibility and EPR spectra proved that $S = 4$ is the ground state. To reproduce the magnetic susceptibility data, we assumed two different exchange interactions in the spin Hamiltonian, possibly a serious simplification in light of the lack of symmetry in our tetrametallic molecule. Broken symmetry DFT calculations, in accordance with the magnetic and EPR data, confirm that the exchange interactions J_1 and J_2 in the system are ferromagnetic and that the magnitude depends on the Ni–O–Ni angles. The ferromagnetic *J* values are smaller with larger Ni–O–Ni angles.

Determination of the exchange coupling constants in nickel(II) cubanes is difficult. In addition to six exchange interactions, which may all be different, the magnetic properties

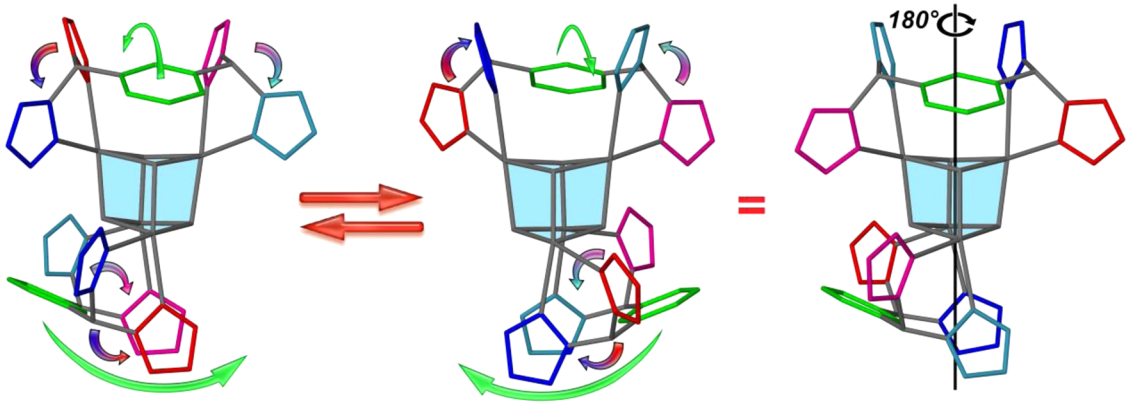

Figure 16. The exchange of the nonequivalent pyrazolyl rings of **3** through a twist of the pyrazolyl rings, accompanied by the 180° flip of the phenylene linkers (left and middle molecules). Rotation of the middle structure by 180°, after both ligands have undergone the Columbia Twist and Flip motion, results in the view on the right side, which is in a similar orientation to the one on the left with the rings and cubane-core positions exchanged.

dx.doi.org/10.1021/ic403013d | *Inorg. Chem.* 2014, 53, 4325–4339

Table 3. Results of the Broken Symmetry DFT Calculations

	1		$[Ni_4L_4(MeOH)_4]\cdot H_2O$[5b]		$[Ni_4(L)_4Cl_4(H_2O)_3(EtOH)]\cdot H_2O$[5c]		F[a]		Br[a]	
Ni−O−Ni angle[b]	98.6	101.1	96.5	100.2	97.2	100.6	97.2	100.6	97.2	100.6
charge on nickel(II)[c]	0.689	0.706	0.828	0.823	0.733	0.732	0.840	0.843	0.722	0.722
charge on O[d]	−0.284	−0.285	−0.804	−0.795	−0.818	−0.808	−0.816	−0.816	−0.816	−0.805
spin density on nickel(II)[c]	1.700	1.709	1.690	1.692	1.684	1.684	1.710	1.713	1.671	1.674
spin density on O[d]	0.110	0.108	0.104	0.108	0.102	0.110	0.092	0.097	0.103	0.112
overlap of the magnetic orbitals	0.039	0.047	0.039	0.048	0.045	0.058	0.041	0.052	0.046	0.052
	0.014	0.016	0.018	0.024	0.016	0.023	0.013	0.022	0.016	0.023
J	12.2	6.8	10.1	−3.4	9.1	2.1	7.6	0.7	9.0	2.0
J_{exp}	9.2	2.1	17.9	−11.2	23.2	2.8				

[a]The F- and Br-containing molecules were generated from the original structure of $[Ni_4(L)_4Cl_4(H_2O)_3(EtOH)]\cdot H_2O$, where HL = (2-pyridyl)methanol.[5c] [b]Average of two Ni−O−Ni angles. [c]Average of two nickel(II) ions. [d]Average of two O atoms.

are also affected by the zfs effects. In some cases the symmetry of the molecule is high enough that the HDVV Hamiltonian can be logically constructed. In one such case, $[Ni_4L_4(MeOH)_4]\cdot H_2O$, where H_2L is a pyrazole-based tridentate diol,[5b] all four nickel(II) ions are symmetry-related and are equivalent. The exchange interactions can be clearly divided into a group of four equal interactions and another group of two, according to

$$\hat{\mathbf{H}}_{HDVV} = -J_1(\hat{\mathbf{S}}_1\hat{\mathbf{S}}_2 + \hat{\mathbf{S}}_1\hat{\mathbf{S}}_3 + \hat{\mathbf{S}}_2\hat{\mathbf{S}}_4 + \hat{\mathbf{S}}_3\hat{\mathbf{S}}_4) - J_2(\hat{\mathbf{S}}_1\hat{\mathbf{S}}_4 + \hat{\mathbf{S}}_2\hat{\mathbf{S}}_3) \quad (6)$$

(note the difference between eq 6 and eq 1). In the group related to J_1, the Ni−O−Ni bond angles (for each interaction) are 97.95° and 95.09°, while in the J_2 group all Ni−O−Ni angles are 100.2°. Interestingly, it was shown that a range of J_1, J_2 pairs give fits of similar quality. Out of these fits, the one being in accord with a postulated J dependence on the Ni−O−Ni angle was chosen.[5b] The J_1 of 17.8 cm^{-1} and J_2 of −11.3 cm^{-1} (converted to the notation used in the present paper) were reported.

In the case of **1**, the cubane molecule has no symmetry. The largest Ni−O−Ni angles reach 101.5°, yet both J_1 and J_2 in Hamiltonian (1) were found to be positive (ferromagnetic). Moreover, in contrast to reference 5b, we do not seem to have a freedom in choosing the J_1, J_2 pairs, and our results vary from the postulated J Ni−O−Ni angle relation.[5b] To get more insight, we performed the broken symmetry DFT calculations in exactly the same way as those for **1** described above for compound $[Ni_4L_4(MeOH)_4]\cdot H_2O$[5b] and another nickel(II) cubane compound, $[Ni_4L_4Cl_4(H_2O)_3(EtOH)]\cdot H_2O$ where HL is (2-pyridyl)methanol,[5c] using crystallographically determined coordinates. The latter complex[5c] contains Cl^- coordinated to nickel(II), and we performed additional calculations with the Cl^- substituted by F^- or Br^- at appropriate distances from nickel(II). Selected results of the broken symmetry DFT calculations are presented in Table 3. In each case (where experimental data exist) we found the same signs for the exchange coupling constant as the ones reported by the authors—two ferromagnetic interactions in our complex **1**, one ferro- and one antiferromagnetic interaction in $[Ni_4L_4(MeOH)_4]\cdot H_2O$[5b], and two ferromagnetic interactions in $[Ni_4(L)_4Cl_4(H_2O)_3(EtOH)]\cdot H_2O$ where HL is (2-pyridyl)-methanol,[5c] the latter in agreement with the original paper, rather than the possible reassessed values in reference 5b. These results suggest that the Ni−O−Ni angle is indeed the most important parameter determining the magnitude and character of the exchange interactions, yet ferromagnetic interactions can be found for Ni−O−Ni angles larger than 100° (see Table 3).

The EPR spectra of **1** at low temperatures (3−30 K) could be satisfactorily simulated using the giant spin Hamiltonian for $S = 4$. The signs of the zfs parameters for $S = 4$ could be determined from the high-field EPR, $D = -0.299$ cm^{-1}, $E = -0.036$ cm^{-1}. However, we are unable to reconcile the EPR and magnetic susceptibility results. The zfs parameters of the giant spin Hamiltonian for the $S = 4$ ground state contain contributions due to the zfs on individual nickel(II) ions, but these contributions depend on the mutual orientations. Another contribution may exist that is related to the anisotropy of the exchange interactions. This contribution is likely less important for the magnetic properties, but it may affect the EPR spectra. An approximation has been used in the literature in which only the zfs splitting of the ground state is taken into account.[5,6a] This approximation works best if the ground state is well-isolated from the excited states. In the case of **1**, this method proved to be not suitable for the magnetic susceptibility calculation, but it is sufficiently good for the calculation of the magnetization at 2 K. At this temperature the EPR parameters could be used (Figure 11, $g_x = 2.205$, $g_y = 2.157$, $g_z = 2.204$, $D = -0.299$ cm^{-1}, $E = -0.036$ cm^{-1}, $B_4^0 = -3.7 \times 10^{-5}$ cm^{-1}, $B_4^2 = 4.2 \times 10^{-4}$ cm^{-1}, $B_4^4 = -1.6 \times 10^{-4}$ cm^{-1}). The DFT calculations of the zfs on individual nickel(II) ions suggest that the zfs is strongly nonaxial with $E/D \approx 0.2$, further complicating the problem. Various assumptions concerning the E/D ratio and the directions of the nickel(II) zfs tensors have only limited effect on the J values calculated from the magnetic susceptibility, and there appears to be no chance to shift the J_2 value into the antiferromagnetic range. Strong sensitivity of the exchange interactions in the nickel(II) cubane complexes to the lattice solvent removal has also been observed.[5] Solvent loss could also have affected our results, although the sample was not vacuum-dried before performing the magnetic susceptibility measurements and elemental analysis indicates that samples dried to constant weight retain the coordinated DMF.

We note that negative D in ferromagnetically coupled transition-metal polymers often leads to the phenomenon of the single-molecule magnetism. In the present case, however, the energy barrier $E = |D|S^2$ is only ~4.8 cm^{-1}, while values on the order of 50 cm^{-1} would be desired.[5o] A nickel(II) cubane has been described showing D in the $S = 4$ state slightly larger than ours, −0.43 cm^{-1} (from magnetic data)[5u] versus our −0.299 cm^{-1} (from high-field EPR), which indeed exhibits the SMM behavior at extremely low temperatures, below 0.4 K.

dx.doi.org/10.1021/ic403013d | Inorg. Chem. 2014, 53, 4325−4339

CONCLUSIONS

We synthesized nickel(II) and cadmium(II) compounds with a cubane core, where the metal centers and the triply bridging hydroxide groups alternate at the eight corners of a cube. This arrangement is supported by a ligand that links two bis(pyrazolyl)methane units by a phenylene spacer $\mathbf{L_m}$, and in the solid state solvent molecules resulting in the formula $[M_4(\mu_3\text{-}OH)_4(\mu\text{-}\mathbf{L_m})_2(solvent)_4](ClO_4)_4$. In contrast, similar synthetic procedures yield dinuclear $[M_2(\mu\text{-}OH)(\mu\text{-}\mathbf{L_m})_2](ClO_4)_3$ for M = Fe(II), Co(II), Cu(II), Zn(II). NMR spectra of the cadmium(II) compound show it retains the cubane structure in solution but undergoes an unusual dynamic rearrangement that equilibrates the pyrazolyl rings, the hydroxide sites and cadmium(II) sites at higher temperatures. We propose that the mechanism for this process is the combined motion of the pyrazolyl rings twisting and phenylene spacers flipping by 180°, the Columbia Twist and Flip mechanism. The magnetic and EPR studies of the nickel(II) analogue revealed an $S = 4$ ground state and angle-dependent exchange interactions of $J_1 = 9.1$ cm^{-1} (97.9 to 99.5°) and $J_2 = 2.1$ cm^{-1} (Ni−O−Ni angles from 100.3 to 101.5°). These results are supported by broken symmetry DFT calculations. High-field EPR measurements allowed the determination of the sign of the zfs parameters in the $S = 4$ state, $D = -0.299$ cm^{-1}, $E = -0.036$ cm^{-1}.

ASSOCIATED CONTENT

Supporting Information

X-ray crystallographic files in CIF format, additional information related to the saturation transfer experiment, Ni−O−Ni bond angles, EPR data, results of the broken symmetry DFT calculations. This material is available free of charge via the Internet at http://pubs.acs.org.

AUTHOR INFORMATION

Corresponding Authors

*E-mail: reger@mailbox.sc.edu. Phone: 803-777-2587. Fax: 803-777-9521. (D.L.R.)

*E-mail: ozarowsk@magnet.fsu.edu. (A.O.)

Notes

The authors declare no competing financial interest.

ACKNOWLEDGMENTS

The authors acknowledge with thanks the financial support of the National Science Foundation (NSF) through Grant CHE-1011736. The high-field EPR spectra were recorded at the National High Magnetic Field Laboratory, which is funded by the NSF through the Cooperative Agreement No. DMR-1157490, the State of Florida, and the Department of Energy. J.J. is grateful to Ministry of Science and Higher Education of the Polish Republic for financial support in the purchase of the Bruker ELEXSYS E 500 EPR spectrometer.

REFERENCES

(1) (a) Halcrow, M. A.; Christou, G. *Chem. Rev.* **1994**, *94*, 2421−2481. (b) Fukuyama, K. *Handbook of Metalloproteins;* Wiley: Chichester, U.K., 2001; 543−552. (c) Carter, C. W. *Handbook of Metalloproteins;* Wiley: Chichester, U.K., 2001, 602−609.

(2) (a) Urdempilleta, M.; Klyatskaya, S.; Cleuziou, J.-P.; Ruben, M.; Wernsdorger, W. *Nat. Mater.* **2011**, *10*, 502−506. (b) Zhu, L.; Yao, K. L.; Liu, Z. L. *Appl. Phys. Lett.* **2010**, *96*, 082115.

(3) Venegas-Yazigi, D.; Cano, J.; Ruiz, E.; Alvarez, S. *Phys. B* **2006**, *384*, 123−125.

(4) (a) Layfield, R. A. *Organometallics* **2014**, DOI: dx.doi.org/10.1021/om401107f. (b) Dey, M.; Gogoi, M. *Angew. Chem., Int. Ed.* **2013**, 12780−12782. (c) Bogni, L.; Wernsdorfer, W. *Nat. Mater.* **2008**, *7*, 179−186. (d) Glaser, T. *Chem. Commun.* **2011**, *47*, 116−130. (e) Affronte, M.; Troiani, F.; Ghirri, A.; Candini, A.; Evangelisti, M.; Corradini, V.; Carretta, S.; Santini, P.; Amoretti, G.; Tuna, F.; Timco, G.; Winpenny, R. E. P. *J. Phys. D: Appl. Phys.* **2007**, *40*, 2999−3004. (f) Enders, A.; Skomski, R.; Honolka, J. *J. Phys.: Condens. Matter* **2010**, *22*, 433001. (g) Miller, J. S. *Dalton Trans.* **2006**, 2742−2749.

(5) Publications listed chronologically: (a) Zhang, S.-H.; Zhang, Y. D.; Zou, H. H.; Guo, J. J.; Li, H. P.; Song, Y.; Liang, H. *Inorg. Chim. Acta* **2013**, *396*, 119−125. (b) Das, A.; Klinke, F. J.; Demeshko, S.; Meyer, S.; Dechert, S.; Meyer, F. *Inorg. Chem.* **2012**, *51*, 8141−8149. (c) Sun, J.-P.; Li, L.-C.; Zheng, X.-Y. *Inorg. Chem. Commun.* **2011**, *14*, 877−881. (d) Feng, X.; Ma, L.-F.; Zhao, J.-S. *Inorg. Chem. Commun.* **2011**, *14*, 584−591. (e) Zhang, W.-H.; Sulaiman, N. B.; Tio, S. P. X.; Hor, A. T. S. *CrystEngComm* **2011**, *13*, 2915−2922. (f) Zhang, S.-H.; Li, N.; Ge, C.-M.; Feng, C.; Ma, L.-F. *Dalton Trans.* **2011**, *40*, 3000−3007. (g) Yu, G.-M.; Zhao, L.; Zou, L.-F.; Guo, Y.-N.; Xu, G.-F.; Li, Y.-H.; Tang, J. *J. Chem. Crystallogr.* **2011**, *41*, 606−609. (h) Wang, F.-M.; Lin, J.-G.; Xing, Y.-Y.; Liu, Y.-M.; Lu, C.-S.; Meng, Q.-J. *J. Coord. Chem.* **2010**, *63*, 3431−3440. (i) Moro, F.; Piga, F.; Krivokapic, I.; Burgess, A.; Lewis, W.; McMaster, J.; van Slageren, J. *Inorg. Chim. Acta* **2010**, *363*, 4329−4336. (j) Fomina, I. G.; Dobrokhotova, Z. V.; Aleksandrov, G. G.; Proshenkina, O. Yu.; Kovba, M. L.; Bogomyakov, A. S.; Ikorskii, V. N.; Novotortsev, V. M.; Eremenko, I. L. *Russ. Chem. Bull., Int. Ed.* **2009**, *58*, 11−20. (k) Mandal, D.; Hong, C. S.; Kim, H. C.; Fun, H.-K.; Ray, D. *Polyhedron* **2008**, *27*, 2372−2378. (l) Lin, Z.; Li, Z.; Zhang, H. *Cryst. Growth Des.* **2007**, *7*, 589−591. (m) Isele, K.; Gigon, F.; Williams, A. F.; Bernardinelli, G.; Franz, P.; Decurtins, S. *Dalton Trans.* **2007**, 332−341. (n) Alley, K. G.; Bircher, R.; Güdel, H. U.; Moubaraki, B.; Murray, K. S.; Abrahams, B. S.; Boskovic, C. *Polyhedron* **2007**, *26*, 369−377. (o) Milios, C. J.; Vinslava, A.; Wernsdorfer, W.; Moggach, S.; Parsons, S.; Perlepes, S. P.; Christou, G.; Brechin, E. K. *J. Am. Chem. Soc.* **2007**, *129*, 2754−2755. (p) Song, X.-Y.; Xu, Y.; Li, L.; Liao, D.; Jiang, Z. *Inorg. Chim. Acta* **2007**, 2039−2044. (q) Abrahams, B. F.; Hudson, T. A.; Robson, R. *Chem.—Eur. J.* **2006**, *12*, 7095−7102. (r) Yang, E.-C.; Wernsdorfer, W.; Zakharov, L. N.; Karaki, Y.; Yamaguchi, A.; Isidro, R. M.; Lu, G.-D.; Wilson, S. A.; Rheingold, A. L.; Ishimoto, H.; Hendrickson, D. N. *Inorg. Chem.* **2006**, *45*, 529−546. (s) Li, Y.-M.; Zhang, J.-J.; Fu, R.-B.; Xiang, S.-C.; Sheng, T.-L.; Yuan, D.-Q.; Huang, X.-H.; Wu, X.-T *Polyhedron* **2006**, *25*, 1618−1624. (t) Sieber, A.; Boskovic, C.; Bircher, R.; Waldmann, O.; Ochsenbein, S. T.; Chaboussant, G.; Güdel, H. U.; Kirchner, N.; van Slageren, J.; Wernsdorfer, W.; Neels, A.; Stoeckli-Evans, H.; Janssen, S.; Juranyi, F.; Mutka, H. *Inorg. Chem.* **2005**, *44*, 4315−4325. (u) Moragues-Canovas, M.; Helliwell, M.; Ricard, L.; Riviere, E.; Wernsdorfer, W.; Brechin, E.; Mallah, T.; Eur, J. *Inorg. Chem.* **2004**, 2219−2222. (v) Yang, E.-C.; Wernsdorfer, W.; Hill, S.; Edwards, R. S.; Nakano, M.; Maccagnano, M.; Zakharov, L. N.; Rheingold, A. L.; Christou, G.; Hendrickson, D. N. *Polyhedron* **2003**, *22*, 1727−1733. (w) Clemente-Juan, J. M.; Chansou, B.; Donnadieu, B.; Tuchagues, J. P. *Inorg. Chem.* **2000**, *39*, 5515−5519. and references therein. (x) Escuer, A.; Font-Bardía, M.; Kumar, S. B.; Solans, X.; Vicente, R. *Polyhedron* **1999**, *18*, 909−914.

(6) (a) Wikstrom, J. P.; Nazarenko, A. Y.; Reif, W. A.; Rybak-Akimova, E. V. *Inorg. Chim. Acta* **2007**, *360*, 3733−3740. (b) Ballester, L.; Coronado, E.; Gutierrez, A.; Monge, A.; Perpinan, M. F.; Pinilla, E.; Rico, T. *Inorg. Chem.* **1992**, *31*, 2053−2056. (c) Boyd, P. D. W.; Martin, R. L.; Schwarzenback, G. *Aust. J. Chem.* **1988**, *41*, 1449−1456. (d) Aurivillius, B. *Acta Chem. Scand.* **1977**, *A31*, 501−508.

(7) (a) Zhu, R.-Q. *Acta Crystallogr.* **2011**, *E67*, m1416−m1416. (b) Lee, C.-J.; Wei, H.-H; Lee, G.-H.; Wang, Y. *Inorg. Chem. Commun.* **2000**, *3*, 690−693.

(8) (a) Chen, Z.; Liang, F.; Zhou, S.; Xia, C.; Hu, R. *J. Mol. Struct.* **2007**, *827*, 20−24. (b) Suen, M.-C.; Wang, J.-C. *Inorg. Chem. Commun.* **2006**, *9*, 478−481. (c) Tong, M.-L.; Lee, H. K.; Zheng, S.-L.; Chen, X.-M. *Chem. Lett.* **1999**, 1087−1088.

(9) (a) Reger, D. L.; Watson, R. P.; Smith, M. D. *Inorg. Chem.* **2006**, *45*, 10077−10087. (b) Reger, D. L.; Foley, E. A.; Watson, R. P.;

Pellechia, P. J.; Smith, M. D.; Grandjean, F.; Long, G. J. *Inorg. Chem.* **2009**, *48*, 10658−10669. (c) Reger, D. L.; Watson, R. P.; Smith, M. D.; Pellechia, P. J. *Organometallics* **2005**, *24*, 1544−1555.
(10) (a) Reger, D. L.; Pascui, A. E.; Pellechia, P. J.; Smith, M. D. *Inorg. Chem.* **2013**, *52*, 11638−11649. (b) Reger, D. L.; Pascui, A. E.; Foley, E. A.; Smith, M. D.; Jezierska, J.; Ozarowski, A. *Inorg. Chem.* **2014**, *53*, 1975−1988.
(11) Jarek, R. L.; Flesher, R. J.; Shin, S. K. *J. Chem. Educ.* **1997**, *74*, 978−982.
(12) (a) Barbour, L. J. *J. Supramol. Chem.* **2003**, *1*, 189−191. (b) *POV-RAY 3.6;* Persistence of Vision Raytracer Pty Ltd: Victoria, Australia, 2006. (c) Laaksonen, L. *gOpenMol;* Center for Scientific Computing: Espoo, Finland, 2005.
(13) *MestReNOVA v.5.2.5;* Mestrelab Research S. L.: A Coruña, Spain 2008.
(14) Hassan, A. K.; Pardi, L. A.; Krzystek, J.; Sienkiewicz, A.; Goy, P.; Rohrer, M.; Brunel, L.-C. *J. Magn. Reson.* **2000**, *142*, 300−312.
(15) (a) O'Connor, C. J. *Prog. Inorg. Chem.* **1982**, *29*, 203−283. (b) Bain, G. A.; Berry, J. F. *J. Chem. Educ.* **2008**, *85*, 532−536.
(16) Wolsey, W. C. *J. Chem. Educ.* **1973**, *50*, A335−A337.
(17) *SMART Version 5.630, SAINT+ Version 6.45;* Bruker Analytical X-ray Systems, Inc.: Madison, WI, 2003.
(18) Sheldrick, G.M., *SHELXTL Version 6.14;* Bruker Analytical X-ray Systems, Inc.: Madison, WI, 2000.
(19) Shannon, R. D. *Acta Crystallogr.* **1976**, *A32*, 751−767.
(20) Steed, J. W.; Atwood, J. L. *Supramolecular Chemistry,* 2nd ed.; John Wiley & Sons: Chichester, U.K., 2009.
(21) Reger, D. L.; Pascui, A. E.; Smith, M. D.; Jezierska, J.; Ozarowski, A. *Inorg. Chem.* **2012**, *51*, 11820−11836.
(22) Gavrilova, A. L.; Qin, C. J.; Sommer, R. D.; Rheingold, A. L.; Bosnich, B. *J. Am. Chem. Soc.* **2002**, *124*, 1714−1722.
(23) Sandström, J. *Dynamic NMR Spectroscopy;* Academic Press: London & New York, 1982.
(24) Marat, K. *SPINWORKS 3 v.3.1.8.2;* University of Manitoba: Winnipeg, Canada, 2011.
(25) (a) Forsén, S.; Hoffman, R. A. *J. Chem. Phys.* **1963**, *39*, 2892−2901. (b) Babailov, S. P.; Krieger, Y. G. *J. Struct. Chem.* **2001**, *42*, 305−308. (c) DiFranco, S. A.; Maciulis, N. A.; Staples, R. J.; Batrice, R. J.; Odom, A. L. *Inorg. Chem.* **2012**, *51*, 1187−1200. (d) Faller, J. W.; Wilt, J. C. *Organometallics* **2005**, *24*, 5076−5083. (e) Ashby, M. D.; Govindan, G. N.; Grafton, A. K. *J. Am. Chem. Soc.* **1994**, *116*, 4801−4809. (f) Wik, B. J.; Lersch, M.; Krivokapic, A.; Tilset, M. *J. Am. Chem. Soc.* **2006**, *128*, 2682−2696. (g) Rybtchinski, B.; Cohen, R.; Ben-David, Y.; Martin, J. M. L.; Milstein, D. *J. Am. Chem. Soc.* **2003**, *125*, 11041−11050.
(26) Telser, J.; Ozarowski, A.; Krzystek, J. *Specialist Periodical Reviews of the RCS: Electron Paramagnetic Resonance* **2012**, *23*, 209−263.
(27) (a) Burdinski, D.; Bill, E.; Birkelbach, F.; Wieghardt, K.; Chaudhuri, P. *Inorg. Chem.* **2001**, *40*, 1160−1166. (b) Semenaka, V. V.; Nesterova, O. V.; Kokozay, V. N.; Dyakonenko, V. V.; Zubatyuk, R. I.; Shishkin, O. V.; Boca, R.; Jezierska, J.; Ozarowski, A. *Inorg. Chem.* **2010**, *49*, 5460−5471.
(28) (a) Abragam, A.; Bleaney, B. *Electron Spin Resonance of Transition Ions;* Clarendon Press: London, U.K., 1970. (b) Bencini, A.; Gatteschi, D. *EPR of Exchange Coupled Systems;* Springer-Verlag: Berlin, Germany, 1990.
(29) (a) Neese, F. *J. Phys. Chem. Solids* **2004**, *65*, 781−785. (b) Maurice, R.; Sivalingam, K.; Ganyushin, D.; Guihery, N.; de Graaf, C.; Neese, F. *Inorg. Chem.* **2011**, *50*, 6229−6236. (c) Onofrio, N.; Mouesca, J.-M. *Inorg. Chem.* **2011**, *50*, 5577−5586. (d) Rodríguez-Fortea, A.; Alemany, P.; Alvarez, S.; Ruiz, E. *Inorg. Chem.* **2002**, *41*, 3769−3778.
(30) Neese, F. The ORCA program system WIREs *Comput. Mol. Sci.* **2012**, *2*, 73−78.
(31) (a) Schaefer, A.; Horn, H.; Ahlrichs, R. *J. Chem. Phys.* **1992**, *97*, 2571−2577. (b) Ahlrichs, R. et al., unpublished. (c) The Ahlrichs auxiliary basis sets were obtained from the TurboMole basis set library under ftp.chemie.uni-karlsruhe.de/pub/jbasen. (d) Eichkorn, K.; Treutler, O.; Ohm, H.; Haser, M.; Ahlrichs, R. *Chem. Phys. Lett.* **1995**, *240*, 283−290. (e) Eichkorn, K.; Weigend, F.; Treutler, O.; Ahlrichs, R. *Theor. Chem. Acc.* **1997**, *97*, 119−124.
(32) (a) Becke, D. A. *Phys. Rev. A: At., Mol., Opt. Phys.* **1988**, *38*, 3098−3100. (b) Perdew, J. P. *Phys. Rev. B* **1986**, *33*, 8822−8824. (c) Perdew, J. P. *Phys. Rev. B* **1986**, *34*, 7406−7406. (d) Kendall, R. A.; Früchtl, H. A. *Theor. Chem. Acc.* **1997**, *97*, 158−163.
(33) Kahn, O.; Briat, B. *J. Chem. Soc., Faraday Trans. 2* **1976**, *72*, 268−281.